TAMPERE UNIVERSITY OF TECHNOLOGY
Department of Electrical Engineering

JULIUS SCHNABEL

COMPENSATION OF PV GENERATOR POWER FLUCTUATIONS USING ENERGY STORAGE SYSTEMS

Master of Science Thesis

Examiner: Prof. Seppo Valkealahti
Examiner and topic approved by the
Faculty Council of the Faculty of
Computing and Electrical Engineering
on 8 April 2015

TIIVISTELMÄ

TAMPEREEN TEKNILLINEN YLIOPISTO
JULIUS SCHNABEL: Compensation of PV Generator Power Fluctuations Using Energy Storage Systems
Diplomityö, 55 sivua, 2 liitesivua
Elokuu 2015
Sähkötekniikan diplomi-insinöörin tutkinto-ohjelma
Pääaine: Uusiutuvat sähköenergiateknologiat
Tarkastaja: professori Seppo Valkealahti
Avainsanat: aurinkosähkö, energiavarasto, sähkön laatu, pätötehon kompensointi.

Todisteet ilmastonmuutoksesta ovat lisänneet kiinnostusta uusiutuvaa energiaa kohtaan. Aurinkosähkö on yksi merkittävimmistä uusiutuvista energian tuotantomuodoista ja jatkuvasti kasvava teollisuuden ala. Aurinkosähkötuotanto on kuitenkin nopeasti ja voimakkaasti vaihtelevaa. Syötettäessä verkkoon paljon voimakkaasti heiluvaa tehoa, on verkon stabiilius vaarassa. Yhä useammat verkko-operaattorit asettavat aurinkosähkön tuotannon heilunnalle rajoituksia.

Tuotantoa tukevien energiavarastojen käyttö on todettu sopivaksi tavaksi tehoheiluntojen kompensointiin. Tämä diplomityö paneutuu energiavarastojen käyttäytymiseen, ohjaukseen ja mitoittamiseen aurinkosähkön asettamien vaatimusten pohjalta. Työssä esitellään yleinen tapa mallintaa aurinkosähkön tuotantoa säteilytehoja lämpötilamittausten avulla. Hyödyntäen mallia ja kattavia mittauksia, työssä tarkastellaan virtuaalisia energiavarastoja aurinkosähkövoimaloiden yhteydessä rajoittumatta mihinkään tiettyyn järjestelmään.

Työn tuloksena todetaan, kuinka energiavaraston tehon ja kapasiteetin tarve on voimakkaasti riippuvainen varaston ohjausmetodista. Huomattavia säästöjä kapasiteettissa voidaan tehdä hyödyntämällä energiavaraston varaustasapainon ylläpitoa. Tämä ohjaustapa voi kuitenkin aiheuttaa ylimääräisiä tuotantokatkoja. Työssä esitellään ja vertaillaan tapoja katkojen välttämiseksi, jotta varaustasapainon hallintaa voidaan hyödyntää.

Työn tuloksista nähdään, kuinka energiavaraston mitoitus riippuu suuresti voimalan koosta ja tehoheilunnan rajoituksesta. Todella tiukat rajat vaativat suhteellisen suuren kapasiteetin riippumatta voimalan koosta. Varaston tehontarve pienenee sekä voimalan koon että heiluntarajan mukaan. Tehontarve pienenee myös, mikäli heiluntarajoja ei tarvitse noudattaa sataprosenttisesti. Työssä todetaan lisäksi, että tehoheilunnan kompensointi aiheuttaa varastolle eksponentiaalisesti laskevan määrän purkaussyklejä kompensointienergian funktiona. Sykleistä seuraava varaston heikentyminen on marginaalisen pientä hyödynnettäessä sopivaa varastotyyppiä.

ABSTRACT

TAMPERE UNIVERSITY OF TECHNOLOGY
JULIUS SCHNABEL: Compensation of PV Generator Power Fluctuations Using Energy Storage Systems
Master's Thesis, 55 pages, 2 appendix pages
August 2015
Master's Degree Program in Electrical Engineering
Major: Renewable Electrical Energy Technologies
Examiner: Professor Seppo Valkealahti
Keywords: photovoltaics, energy storage, power quality, active power compensation.

General awareness of global warming has increased interest towards renewable energy solutions. Photovoltaic solar power is one of the most notable renewable energy production methods and a continuously increasing industry. The power production behavior of photovoltaics, however, is rapidly and intensively fluctuating even on very short timescales. Feeding such fluctuating power into a power system can cause serious stability issues. More and more grid operators are demanding solar power producers to regulate the fluctuations to stay within strict ramp rate limits.

Energy storage systems have been recognized as a viable solution for compensating these fluctuations. This thesis delves into the behavior, control and sizing of these systems based on the requirements that the compensation application sets for them. The thesis depicts how solar power can be generally modelled with irradiance and temperature measurements. The model is utilized together with extensive measurement data to study virtual energy storage systems with solar power plants.

This thesis demonstrates how the capacity and power requirements of the energy storage are highly dependent on the control method of the system. Notable capacity savings can be made by utilizing state of charge control. The control, however, can cause production outages. Methods to reduce these outages are presented in this thesis in order to enable the use and benefits of state of charge control.

The results of this thesis show how the sizing of the storage depends greatly on the size of the plant and the required ramp rate limit. Very strict ramp rate limits require the storage capacity to be relatively high regardless of the plant size. The storage power requirement is inversely proportional to both the generator size and ramp rate limit. Power rating savings can also be made if complete ramp rate limit obedience is not necessary. The thesis also reveals how the fluctuation compensation induces an exponentially decreasing amount of stress to the storage as a function of the required compensation energy. The degradation resulting from the stress is shown to be minimal if an appropriate storage technology is utilized.

PREFACE

This Master of Science thesis was done for the Department of Electrical engineering of the Tampere University of Technology. The thesis was part of a project called Solar Energy Systems Project 2 (SESPRO2) done in co-operation with ABB Ltd. Finland. The examiner of the thesis was professor Seppo Valkealahti. The topic of the thesis was suggested by ABB representatives and further detailed by professors Valkealahti and Teuvo Suntio.

I want to express my gratitude to the SESPRO2-project team: M.Sc. Aapo Aapro, M.Sc. Juha Jokipii, M.Sc. Jyri Kivimäki, M.Sc. Kari Lappalainen, Ph.D. Tuomas Messo, M.Sc. Jukka Viinamäki and the professors Valkealahti and Suntio for all the guidance and support they have given me related to this thesis. B.Sc. Antti Hilden, B.Sc. Matti Marjanen, M.Sc. Jenni Rekola and all the other department colleagues also deserve my thanks for providing a lenient, supportive and comfortable working environment. Special thanks goes to my friends and family for all the support and friendship they have given me in the past five years leading to this thesis.

Tampere, August 18, 2015

Julius Schnabel

CONTENTS

LIST OF SYMBOLS AND ABBREVIATIONS

ABBREVIATIONS

AC	Alternating Current
CAES	Compressed Air Energy Storage
CCR	Constant Current Region
CVR	Constant Voltage Region
DC	Direct Current
DoD	Depth of Discharge
ESS	Energy Storage System
EoL	End of Life
IV	Current-voltage
MPP	Maximum Power Point
MPPT	Maximum Power Point Tracking
OC	Open-circuit
PHS	Pumped Hydro Storage
PoA	Plane of Array
PV	Photovoltaic
PVG	Photovoltaic Generator
RMSD	Root Mean Square Difference
RR	Ramp Rate
SC	Short-circuit
SMES	Super Magnetic Energy Storage
SoC	State of Charge
STATCOM	Static Synchronous Compensator
STC	Standard Testing Conditions
STD	Standard Deviation
SVC	Static VAR Compensator
TUT	Tampere University of Technology
WVM	Wavelet Variability Model

SYMBOLS

A	Area
C_{deg}	Capacity degradation
C_{ESS}	Energy storage system capacity
d	Square PVG area side dimension
D	Extreme ramp rate difference
E_{error}	Difference of measured and reference energy
E_{ESS}	Energy state of an energy storage system
G	Irradiance
G_{s}	Spatial irradiance
G_{STC}	Irradiance in standard testing conditions
I	Current
I_{SC}	Short-circuit current
K	P-controller proportional gain
N	Cycle count number

N_{DoD}	Cycle count number for a given depth of discharge
P	Power
P_{ESS}	Charge and discharge power of an energy storage system
P_{grid}	Power fed into the grid
P_{mod}	Modelled power
P_{MPP}	Power at the maximum power point
P_{PVG}	Power produced by a photovoltaic generator
P_{SoC}	State of Charge balancing power
r	Ramp rate limit
s	Laplace operator
R_{ext}	External Resistance
T	Temperature
T_{STC}	Temperature in standard testing conditions
t	Time operator
t_{out}	Production outage time
V	Voltage
V_{OC}	Open-circuit voltage
v_{c}	Cloud speed
Δt	Time step

SUBSCRIPTS

max	Refers to a maximum value
min	Refers to a minimum value
nom	Refers to a nominal value
obs	Refers to an observed value
ref	Refers to a reference value

1. INTRODUCTION

The 21st century climate issues and the awareness of how to combat them have created a demand for clean and renewable energy [1]. Photovoltaic (PV) solar energy is one of the most promising renewable energy sources and an increasing industry. The cumulative global PV capacity has grown at an approximate rate of 49 % per year since 2003. A clear majority of this capacity is grid-connected, providing electricity to power systems around the world. [2]

Although renewable and self-sufficient, PV power production is highly volatile. Irregular and quickly changing cloud shadows can cause rapid and intensive fluctuations to a PV Generator's (PVG) power output. If injected to a public power system in large scale such fluctuations can cause frequency instability issues [3]. Compared to conventional energy sources the amount of grid-connected PV systems has been relative low prior to this decade. The amount of fluctuations injected to public grids has previously been low enough to be absorbed and smoothed by the inertia within the power systems. As the amount of grid-connected PV systems has increased so have the concerns of the effect of fluctuation on power system stability.

Frequency instability is first and foremost a power quality issue. In order to guarantee good power quality in their systems, power system operators have begun to impose regulation on PV variability through Ramp Rate (RR) limits [4–8]. In order for PV utilities to comply with these limits PV fluctuations need to be fully controllable. A PV system by itself cannot regulate all of its power fluctuations. An auxiliary Energy Storage System (ESS) could be utilized as an active power compensation unit interconnected to the PV system. However, the addition of auxiliary units to an already expensive system creates additional costs that require minimizing. PV utilities and system suppliers are therefore very interested in the minimum sizing of these storage systems.

This thesis aims to contribute to these issues by examining the PV fluctuation compensation application and the requirements it imposes on an ESS. The focus of the thesis is to derive guidelines for sizing an ESS for this application in Northern European conditions. The main areas of interest are the capacity and power required as well as cycling induced lifetime considerations. Effects of PVG size, ESS control and ramp rate limits are also investigated. The thesis aims to provide general results that are applicable to a wide variety of PV and energy storage systems.

The thesis guides the reader through basic information about PV systems in Chapter 2. PV variability, its effect on power system stability and its compensation with energy storage systems are discussed briefly in Chapter 3. The results of this thesis rely on extensive measurements obtained from Tampere University of Technology (TUT) Solar PV Power Station Research Plant [9]. Chapter 4 presents the plant and its measurements in detail. The general examination of various PV systems is achieved with a PV power output model which is presented and verified in Chapter 5. Finally in Chapter 6 the model is used together with the measurement data to simulate virtual systems of coupled PV and ESS units in year long operation. The ESS is left arbitrary without any restrictions to observe the behavior and derive conclusions about control and sizing.

2. PHOTOVOLTAIC SYSTEMS

This chapter gives insight to the basic operating principles of harnessing solar energy with photovoltaic systems. Solar energy originates from the nuclear reactions within the Sun. The surface of the Sun transfers the nuclear energy further into space by emitting high energy radiation. This solar radiation is the original source of almost all the energy cycling within Earth.

Solar radiation can be assumed to travel to Earth as parallel rays. A common way to interpret the intensity of solar radiation, is to measure the power per unit area that the incoming rays inflict on a plane perpendicular to them. This measure is referred to as irradiance G. The irradiance reaching the outer surface of Earth's atmosphere is approximately constant 1,366 W/m^2 [10]. Molecules within the atmosphere absorb some of the energy of the rays. Clouds especially can block the incoming rays and significantly reduce the amount of irradiance hitting the ground. Solar rays can hit the ground or ground objects directly or indirectly after reflecting from other objects. The combination of both direct and indirect irradiance is the base source of photovoltaic solar energy generation.

2.1 Photovoltaics

A photovoltaic cell is a semiconductor device that converts energy from solar radiation into electrical energy via a phenomenon called the photoelectric effect. The energy of the radiation excites the weakly bonded electrons in the PV cell material, breaking the atomic bonds they form and freeing them from the crystal structure of the cell material. Free electrons are able to travel within the crystal structure, i.e. conduct electric current I.

The photoelectric effect can be further explained with the energy band concept. All the possible energy levels of electrons in an atomic structure are quantized states, which can be grouped together to form so called energy bands. In the structure only two electrons with opposing spin quantum numbers can occupy the same energy level and the bands may house only a set number of electrons. The outermost band full with electrons is called the valence band. Electrons in this band form the atomic bonds and cannot move within the atomic structure. The band with the next highest energy levels is called the conduction band. The conduction band is never full, thus offering unoccupied energy states, i.e. holes, for the conduction electrons to travel

into. These two bands are intervened by an energy state, called the band gap, which no electron may reside in. The band gap is characterized as a specific amount of excitation energy that a valence electron needs in order to phase to the conduction band. [11]

Based on its ability to conduct electricity, any material can be categorized as an insulator, semiconductor or a conductor. Figure 2.1 illustrates the energy band differences between these three categories. A conductor has electrons in the conduction band even at absolute zero temperature. Thus, it is ready for current flow without any additional excitation. An insulator has a full valence band at zero Kelvin, but a large band gap. Thus insulators require excessive amounts of excitation energy before any current flow within the material is possible. A semiconductor, such as used in PV cells, is similar to an insulator but with a much smaller band gap. It can be excited to allow valance electron excitation with solar radiation for instance. However, once excited the electrons quickly exhaust their excitation energy and fall back into the valance band in a phenomenon called recombination.

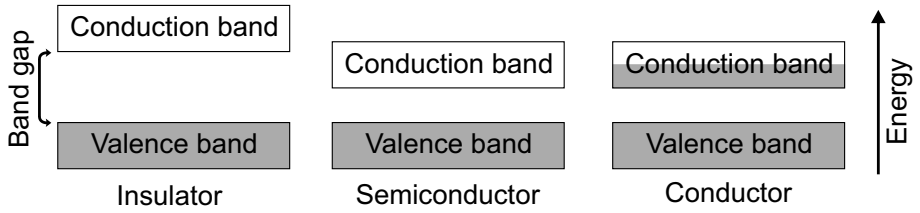

Figure 2.1. Energy band illustration of an insulator, a semiconductor and a conductor. The gray filling represents electrons and the white filling holes occupying the bands.

The conductivity of semiconductors can be further enhanced with doping. Doping means mixing a semiconductor material e.g. silicon with a small amount of specific impurities such as phosphorous or boron atoms. Without the impurities the silicon atoms have a specific amount of outermost electrons to form an even number of binding electron pair bonds, i.e. covalent bonds. When the impurities with different number of outermost electrons form covalent bonds with silicon atoms, they leave excess donor electrons or acceptor holes into the structure as show in Figure 2.2. These donors and acceptors are more readily utilizable for current flow. In the energy band concept they can be characterized as electrons slightly below the conduction band (donor) or holes above the valance band (acceptor). In the charge convention doped semiconductors have either additional negative charge from the donors (n-type), or additional positive charge from the acceptors (p-type). [11]

Even with doped semiconductors the recombination of excited electrons hinders the accumulation of charge. Traditional PV cells utilize the combination of both p and n-type semiconductors in a pn-junction [11]. In the junction region the donor

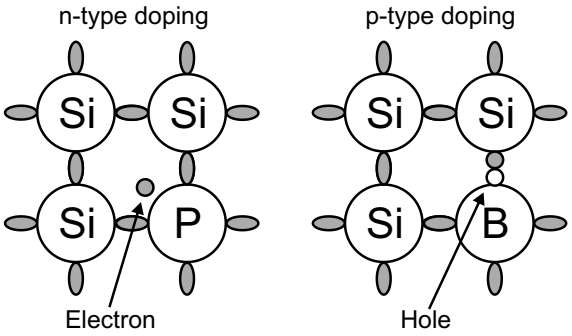

Figure 2.2. The doping of n and p-type silicon semiconductors with phosphorous (left) and boron (right). The resulting donor electron and acceptor hole have been pointed out.

electrons diffuse from the n-side towards the acceptor holes in the p-side, leaving behind positive charge and creating negative charge at the other end. These charges form an electric field over the junction, which tries to separate all electron-hole pairs within the junction. This results in a drift current that opposes the diffuse current. Eventually a balance is met between the opposing currents. Figure 2.3 illustrates the pn-junction and the different charge carrier currents in it.

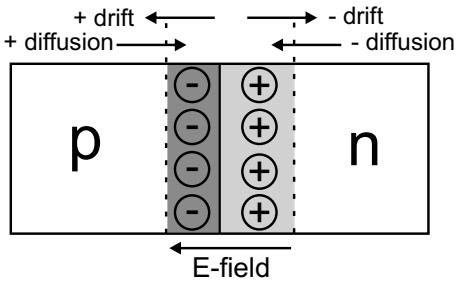

Figure 2.3. A pn-junction and the diffuse and drift currents of electrons (-) and holes (+).

When a PV cell's pn-junction is irradiated new electron-hole pairs are born in the junction and then separated by the electric field. This accumulates opposing charge on both ends of the junction forming positive and negative leads with a voltage V between them. If the leads are not externally joined, i.e. the circuit is open, then the voltage accumulates to a certain maximum. If the leads are joined with an external circuit the separated electrons and holes in the cell have an external route for recombination. The amount of irradiation determines the amount of created charge, whereas the resistivity of the external circuit R_{ext} determines the rate of its discharge, i.e. the amount of current in the external circuit. Figure 2.4 illustrates this concept.

A PV cell has a unique non-linear current-voltage-relationship best illustrated with a current-voltage-curve (IV-curve) show in Figure 2.5. The figure shows how

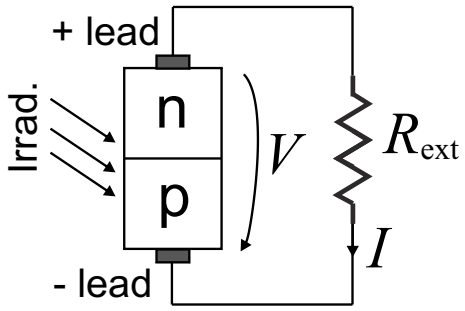

Figure 2.4. A pn-junction within an irradiated PV cell connected to a resistive external circuit.

with infinite, in practice very high, external resistance between the leads, the current is 0 A and the voltage is at its maximum. This state is called open-circuit (OC), hence the voltage in this state is called the open-circuit voltage V_{OC}. When the resistance between the leads is lowered the voltage decreases only moderately while the current increases prominently. At a specific level of external resistance the situation is reversed and the voltage decreases more drastically while the current increase is marginal. When the external resistance is very small the voltage is at zero and the current is at its maximum. This state is called the short-circuit (SC), and hence the current in this state is called the short-circuit current I_{SC}.

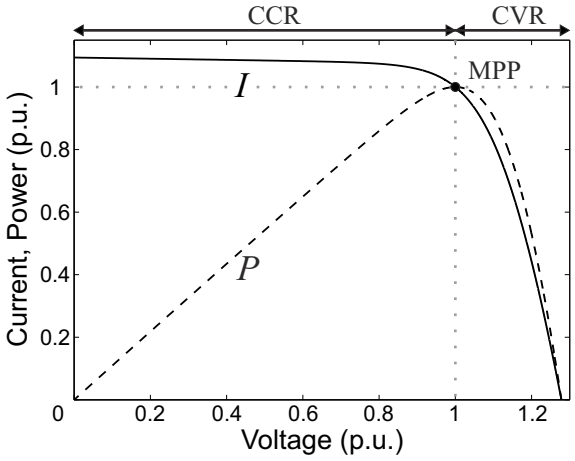

Figure 2.5. An arbitrary PV cell current-voltage-curve (solid) and power-voltage-curve (dashed). The per unit values are in respect to nominal operating conditions.

The dashed line in Fig. 2.5 depicts the power P behaviour resulting from the IV-curve. Maximum power is clearly met at the knee-point where both I and V are largest in respect to each other. This knee-point is called the Maximum Power Point (MPP). The MPP is at the intersection of two other operating regions called the Constant Voltage Region (CVR) and the Constant Current Region (CCR). The operating point of the cell can be changed between CCR, MPP and CVR by externally altering either the output current or the voltage of the cell. For power production

purposes the desirable operating point is clearly the MPP. An attempt to externally alter the operating point in order to reach the MPP is called Maximum Power Point Tracking (MPPT) [10, 12].

2.2 Effect of Operating Conditions

The output of a PV cell is greatly dependent on its operating conditions. The two biggest conditional factors are the cell temperature T and the incident irradiance G [10]. The conditional effects can be simplified to: G mostly affecting I_{SC} directly and T mostly affecting V_{OC} inversely. All the operating points of a PV cell reside between the OC and SC extremes, and are thus affected by T and G respectively to I_{SC} and V_{OC}. Figure 2.6 displays both the irradiance and temperature effects on the IV behavior of a PV cell.

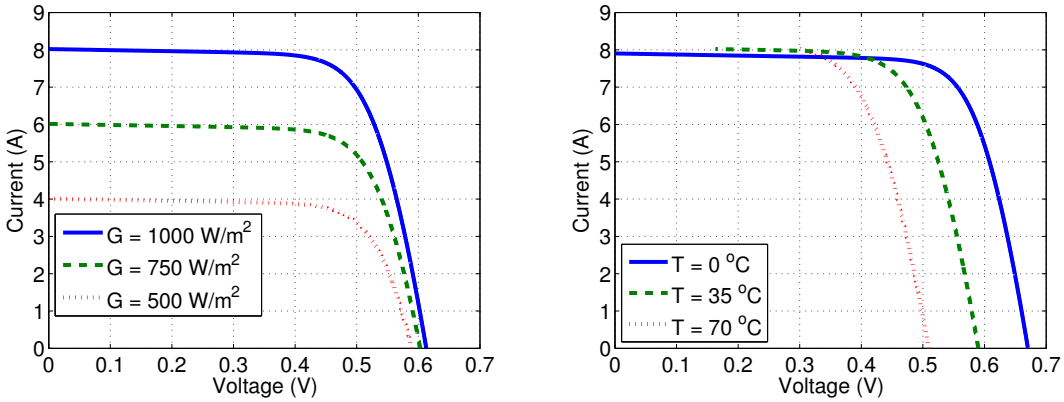

Figure 2.6. A crystalline silicon PV cell IV-curves showing (a) the effect of irradiance while $T = 25$ °C and (b) the temperature effect while $G = 1000$ W/m^2.

Fig. 2.6a shows clearly how increasing the irradiance increases V_{OC} only a little but I_{SC} significantly. Conversely, Fig. 2.6b depicts how the increase of cell temperature marginally increases I_{SC} but has a notable decreasing effect on V_{OC}. Figure 2.7 shows another representation of exactly the same effects. The figure has been depicted relative to common reference conditions called the Standard Testing Conditions (STC), which equal to: air-mass of 1.5, irradiance of 1000 W/m^2 and cell temperature of 25 °C [10]. Although these conditions are not likely met in actual operation they form an adequate baseline for PV cell performance comparisons.

Comparing the ratios at which G and T affect the cell current and voltage in Fig. 2.7, the irradiance has a stronger effect. Additionally, considering that the irradiance can change very rapidly while the changes in cell temperature always have some delay due to thermal inertia, the voltage of a PV cell does not change as fast as the current. For this reason MPPT is commonly realized by controlling

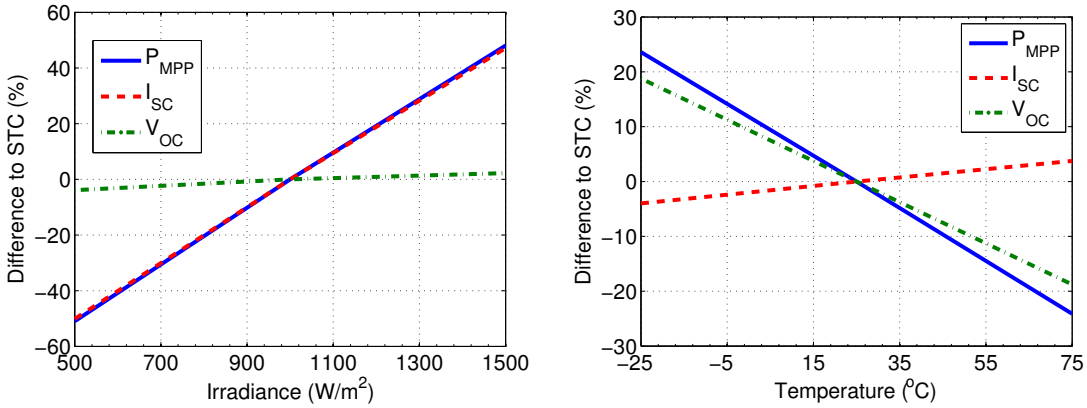

Figure 2.7. STC relative effect of (a) irradiance and (b) temperature on a crystalline silicon PV cell maximum power, OC voltage and SC current.

the cell voltage rather than the current. This approach allows more leniency for the tracking algorithm. [12]

In addition to I_{SC} and V_{OC} Fig. 2.7 also shows how the maximum power P_{MPP} depends on these conditions. Fig. 2.7a displays how the maximum power has almost identical irradiance dependency as the SC current. If the changes in irradiance are also referenced to STC then the dependency has a 1:1 ratio. This indicates that PV cell power could be approximated with just irradiance information. Fig. 2.7b in turn shows how the maximum power decreases approximately 0.5 % per each degree [10]. This reduction is notable, but not as significant to power production as reductions in irradiance.

2.3 PV System Configurations

The basic building blocks of PV systems are PV cells. For instance a typical crystalline silicon cell is a small, approximately 20 cm x 20 cm semiconductor wafer with low current and voltage range. In order to get more practical ouput levels several PV cells can be connected together to create larger PV units called modules. Similarly several modules can be connected together to create PV arrays and array ensembles to create photovoltaic generators.

PV units can be connected together in series or in parallel. Series connection of two identical PV cells operating in identical conditions results in a doubled V_{OC}, while I_{SC} stays the same. Conversely a parallel connection of these cells yields a doubled I_{SC} while V_{OC} remains unchanged. [10] Increasing the number of interconnected cells increases the voltage, current and power range of the whole system. For example the NAPS NP190GKg modules used in the TUT research plant utilize 54 series connected cells to increase the nominal V_{OC} range from 0.6 V to 33 V while

increasing the nominal MPP from 3.5 W to 190 W [9]. Figure 2.8 displays the IV-curve representation of series and parallel connections of two identical PV cells.

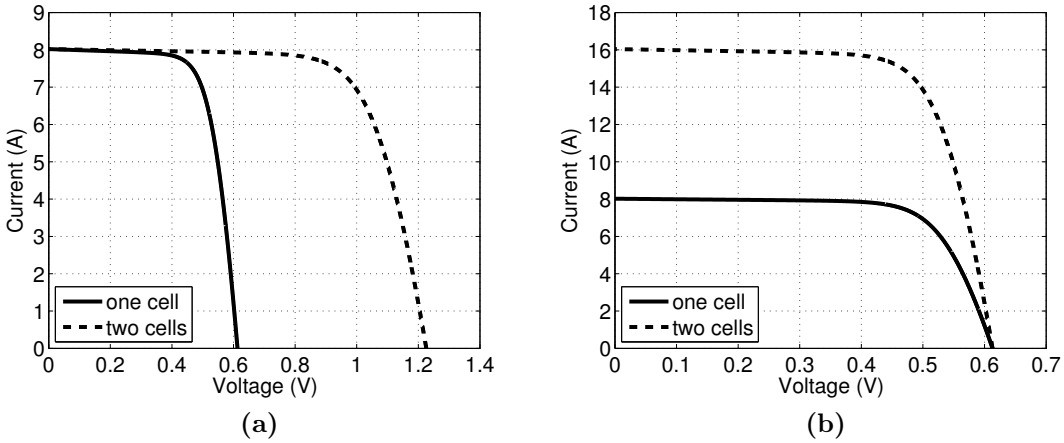

Figure 2.8. IV-curves of two identical PV cells connected in (a) series and (b) parallel in uniform STC conditions.

Series connection of PV cells in asymmetric irradiance conditions, i.e. partial shading or mismatch conditions, proposes a problem however. The current of a multi-cell series connection is determined by the current of the least irradiated cell, which can waste some of the energy generated in the irradiated cell. Additionally, if a series connection of shaded and irradiated cells is short-circuited, the shaded cells dissipate all the power that the irradiated cells would generate. This mechanism can easily destroy the shaded cells. As a protective countermeasure a bypass diode can be connected anti-parallel to the cells. [10] Figure 2.9 shows an example of a bypass diode utilized in a series connection of an irradiated and a shaded cell.

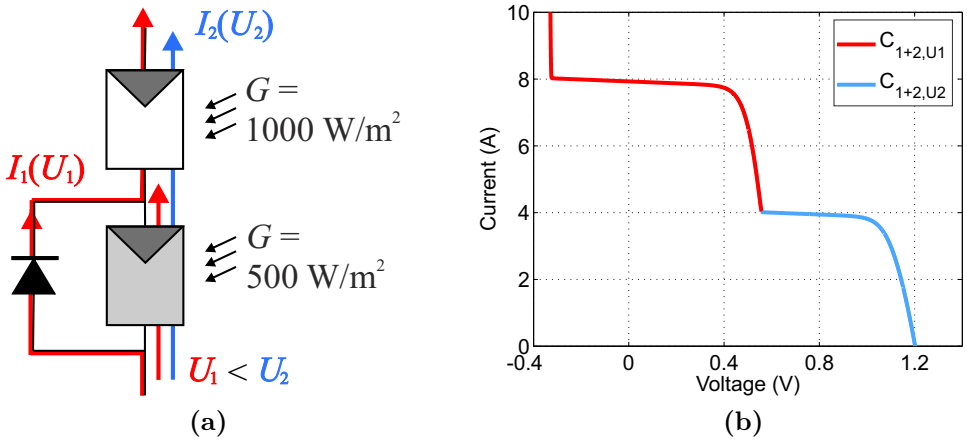

Figure 2.9. Utilization of a bypass diode depicted with (a) the route of the currents with different voltages and (b) the IV behavior of the series connection.

At low voltages the system has a high current generated by the fully irradiated cell. The shaded cell provides what it can of this current, while the diode allows a bypassing route for the rest of the current. At high voltages both cells can generate the same low current and the diode is bypassed in turn. This configuration allows the utilization of the irradiated cells and lowers the amount of dissipated power in a short-circuit. However, it also enables the system to have several MPPs, which complicates MPPT. Typically, PV modules have bypass diodes for groups of 12-24 cells in order to assure overheating protection with minimum amount of components. [10]

By mixing series and parallel connections of smaller PV units, the output of the whole system can be fitted to desired levels. For example a typical array topology has several series connected modules forming strings. Strings in turn can be connected in parallel. In such topology the voltage range of the system can be influenced with the number of modules within the strings, while the current range can be influenced with the number of parallel strings. This configuration requires blocking diodes at the end of each string in order to assure that the current travels to the array terminals in asymmetric conditions. Other more complicated configurations exist to counter problems surfacing from asymmetric conditions, but they are less common and have their individual drawbacks. [10]

A PVG by itself cannot be properly utilized for energy production without a power electronic converter working as an interfacing unit. In direct current (DC) applications the load forces a constant voltage level that drives the PVG to operate at a disadvantageous point. Thus, a DC/DC converter, able to produce a constant output even with varying input, can be used to control the PVG's operating point, while providing the load with a constant voltage. In alternating current (AC) applications the DC output of a PVG has to be inverter into AC with a specific amplitude and frequency. A DC/AC converter (inverter) can be utilized for this purpose to produce a steady AC output while also controlling the variable DC input. AC applications can also utilize the option of a two-staged conversion with the series connection of a DC/DC and DC/AC converters. This set-up broadens the effective PVG operation range for AC applications. [12, 13]

Grid-connected PV systems can be realized with several different interfacing topologies such as the central inverter, string inverter, team concept, two-stage multi-string inverter and the module inverter [14]. Figure 2.10 displays schematics of a few typical topologies. The most common topology is the central inverter, in which several strings are parallel connected to the same inverter. It requires the least amount of components and thus its costs are low and the concept is simple. Its drawback is the low efficiency of centralized MPPT of several modules operating in different conditions [12]. The other interfacing topologies try to address this

problem by further dividing the system into subsystems with individual converters controlling smaller groups of modules. The clear drawbacks of these topologies are the opposites of the benefits of the central inverter topology: high costs and complicated systems.

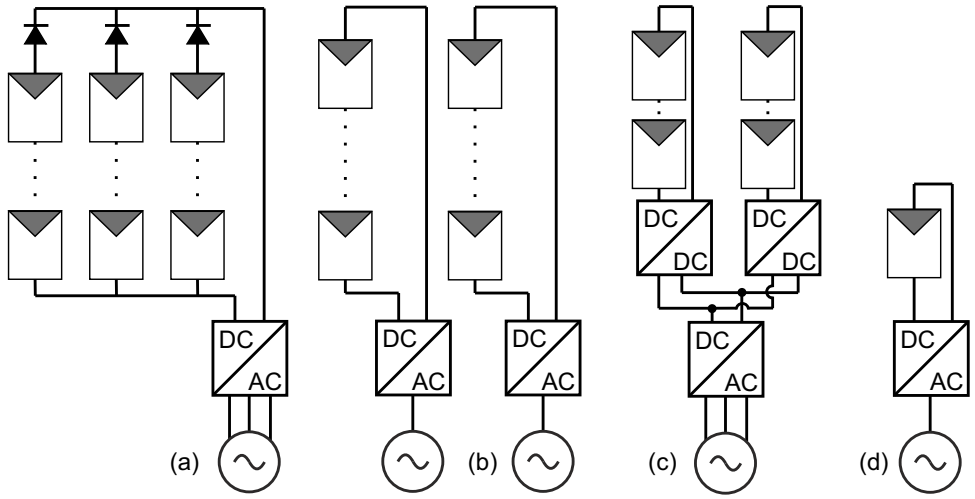

Figure 2.10. Some PVG grid interfacing topologies: (a) central inverter, (b) string inverter, (c) two-stage multi-string inverter, (d) module inverter.

3. COMPENSATING PV FLUCTUATIONS WITH ENERGY STORAGE SYSTEMS

This chapter examines the fluctuations of PV generation, its effect on the power system stability and its compensation with energy storage systems. PV fluctuations refer to the PVG power P_{PVG} falls and rises, sometimes referred to as PV variability as well. Because of the direct irradiance dependency of PVG power, as was shown in Ch. 2.2, PV variability can also be effectively examined via irradiance fluctuations.

3.1 PV Fluctuations

The intermittency of PV is general knowledge, but the general public usually considers PV variability only as the diurnal and seasonal changes. In reality PV variability is also observed as very fast fluctuations caused by clouds shadowing a PVG. Figure 3.1 shows examples of a 3.2 kWp PVG power output on a typical cloudy day in different timescales measured with one second intervals. The high occurrence frequency, amplitude and short durations of fluctuations is evident in the figure.

PV variability can be measured through the concept of fluctuation ramp rates. Momentary PVG power ramp rates can be defined with:

$$\Delta P_{\mathrm{PVG}}(t) = \frac{P_{\mathrm{PVG}}(t) - P_{\mathrm{PVG}}(t - \Delta t)}{\Delta t}, \tag{3.1}$$

where t refers to the current time step, $t - \Delta t$ to the previous time step and Δt to the sampling interval. The results of equation 3.1 are strongly dependent on the sampling interval, and thus aliasing can occur. Nevertheless, this method can give sufficient indications of fluctuation impact if used with a small Δt. Furthermore, a study done in [15] investigated the amount of error using this equation and deemed it small.

PV variability has been extensively researched through both PVG power and irradiance measurements and simulations [15, 16]. Since a RR depends on the used Δt various different results have been reported. Nonetheless, a general consensus of ramp rates being able to reach extreme levels has been established. As an example the maximum one second RR observed in the day depicted in Fig. 3.1a is as high as 40 %/s of the generator's nominal power rating. Extreme RRs measured with large Δt are most of the time only momentary partials of a larger ramp. Although

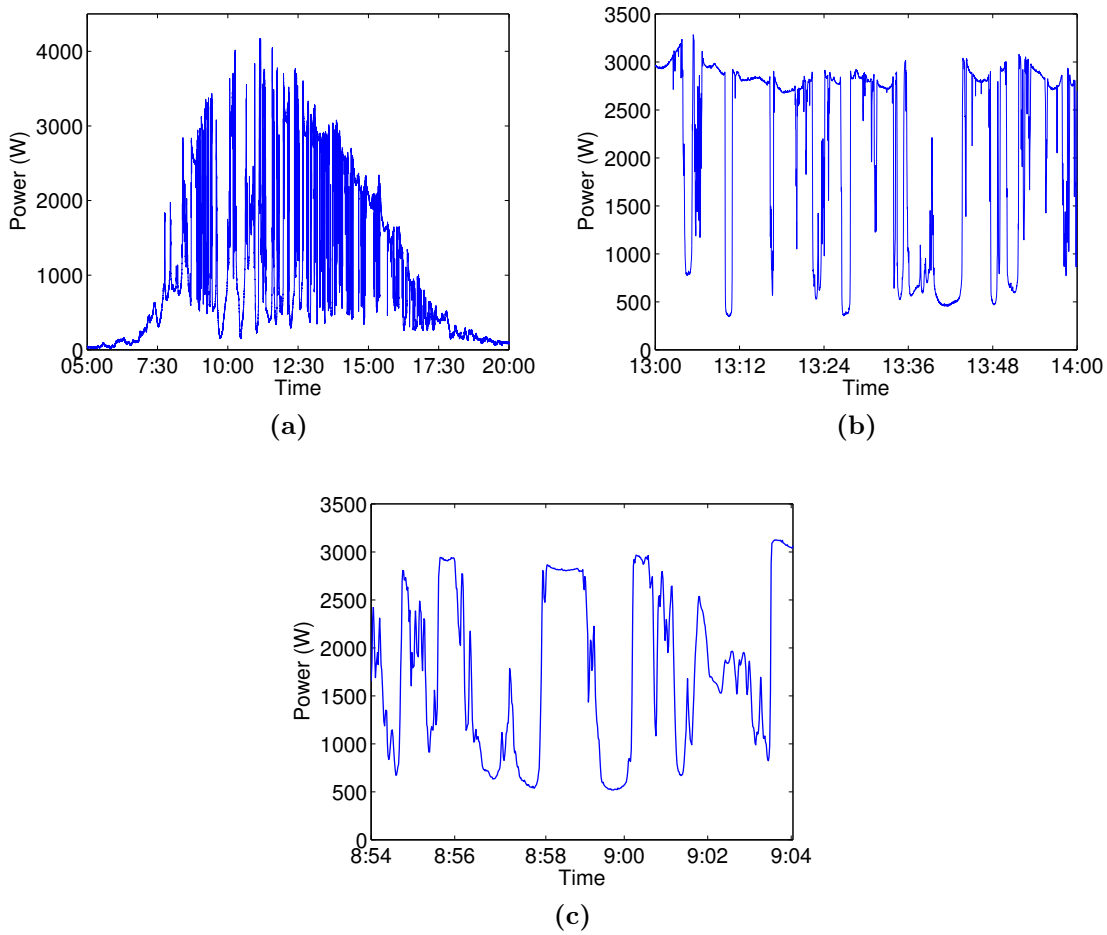

Figure 3.1. An example 3.2 kWp PVG power evolution during a period of (a) the whole day, (b) one hour and (c) 10 minutes observed in the TUT research plant on 15.06.2015.

smaller than the maximum RR, the overall average RR of a fluctuation can still be significantly large. For example several ramps in Fig. 3.1c slope up and down approximately 80 % of the generator's nominal rating in 9-12 seconds, corresponding to an average RR of 6.9 - 8.9 %/s.

It should be noted that PV variability and RRs are also highly dependent on the PVG size, due to spatial smoothing [15–18]. Shortly put: widespread PVGs and dispersed PVG fleets observe a smoother spatial aggregate irradiance and produce smoother total power outputs. This mechanism, however, does not reduce fluctuations indefinitely or propose a valid solutions for fluctuation compensation in all cases. This matter is further discussed in chapter 5.

3.2 Power System Stability

Balance between generation and consumption of power is probably the most vital requirement for any power system. By upholding this balance the frequency of the system can be kept constant. Frequency stability depends on the power system's ability to sustain a steady frequency even when there is significant imbalance in generation and consumption [19]. The most basic way to uphold frequency stability is to have a lot inertia in the system from synchronous generators. PV is often connected to a power system via a converter which has no inertia. Replacing synchronous generators with PV reduces the total system inertia and thus increases the system's sensitivity to frequency deviations. Frequency stability is a significant issue especially in weak and island grids due to low amount of inertia in these systems. [20]

It is important to understand that variability is an innate characteristic of power systems. Loads, power lines, and generators all have some degree of variability. This variability is managed and kept minimum with regulation and careful planning. Variability management is an issue of timescale. In an hours to days timescale, power utilities will commit units to meet expected loads. In a shorter 10 min to hours timescale system operators will alter the output of some of the committed units to follow the changes in consumption. In the shorter than 10 min timescale, system operators schedule regulation reserves to track minute by minute changes in the balance between generation and consumption. Whatever fast variation the system operator cannot counter is usually absorbed by the inertia of the system, resulting in only harmlessly small frequency deviations. [20] Figure 3.2 demonstrates how a daily load balance is kept in a power system with and without fluctuating PV generation.

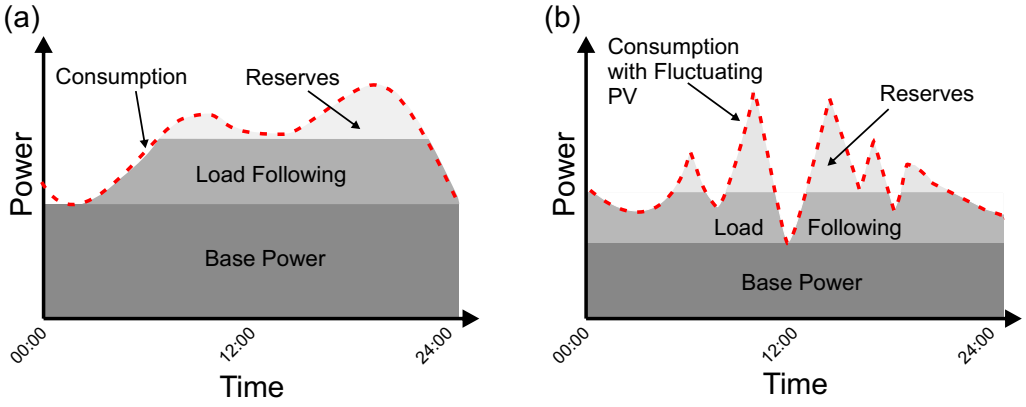

Figure 3.2. The concept of daily power system load profile (a) without and (b) with a lot of fluctuating PV generation.

Although variability is already foreseen and managed in power systems the variability of PV generation proposes some problems. PV generation is foreseeable up

to some degree. Different forecasting horizons from weeks to hours exists and with now-casting temporal resolutions of 10 to 15 minutes are achievable [21]. With these forecasts PV utilities can inform the system operator about the upcoming changes so that other units can be turned on or off to compensate the PV power deficiency or surplus as show in Fig. 3.2b. The occurrence frequency of fluctuations, however, can be very high as Fig. 3.1 shows. Constantly turning reserve plants on and off is not a viable or sustainable solution. The more PV penetration there is, the more the rest of the power system has to adapt to it by keeping more and more responsive reserves on standby.

Power quality wise the bigger issues is the speed of the fluctuations. Current forecasting methods cannot see extremely fast changes. Additionally, traditional frequency regulation reserves are not fast enough to be able to counter such changes. With high enough PV penetration in a system, these fast fluctuations are not absorbed by the system inertia, which leads to frequency instability before the system operator can react to it. Off-nominal frequencies can cause flickering in lighting and malfunctions in interconnected synchronous generators and transformers within the power system. In the worst case scenario damages can be mitigated by disconnecting the fluctuating PV plant and compensating with reserves. This ultimately leads to added costs for the liable PV utility. [20]

3.3 PV Variability Regulation

Many system operators have realized the issue in PV variability and are taking precautionary measures to ensure good power quality in their systems. One of the easiest ways to deal with this problem is to investigate the amount of acceptable PV variability in the system and limit the amount of connected PV units or curtail PV generation respectively [22]. Due to the amount and intensity of PV variability these limits can be relatively low, especially in weak or island grids. This approach is clearly not supportive of the PV industry or global renewable energy goals.

Another more productive way for system operators to regulate the amount of PV variability is to impose limits for the variability itself. Many operators around the world have decreed different ramp rate limits r for PV and other renewable generation in their grid codes. If the system operator can assume that the fastest changes from a PV utility stay within reasonable limits load following and reserve committing becomes much more easier. An often cited case of a PV specific RR limit is the Puerto Rico Power Authority's regulation of 10 %/min of the plant's nominal power. [4]. Similar limits are popular in many other grid codes. Other examples are e.g. 1-30 MW/min in Ireland and 2-10 MW/min in Hawaii depending on the generator size. Some operators specify that the limit concerns only the upward ramps, resulting from the increase of resources, while others require both up- and

downward ramps to be limited. In this thesis all examined RR limits concern both ramp directions. [5–8]

Many of the RR limits are specified in the per-minute convention which gives some room for interpretation. The limit could be seen absolute, meaning that no matter what timescale is used the same rate applies constantly. For example a 10 %/min limit would be interpreted as 0.167 %/s, or 600 %/h and applied at all times. Other ways to interpret the same limit is to look only at the rate of change between 60 second samples or the mean value of a 60 second moving average. In this thesis, however, the limits are assumed to be absolute, and applied at all times.

3.4 Energy Storage System Utilization

In order to comply with the RR limits the PV utilities need to be able to compensate the power fluctuation of their PVGs. Grid-interfacing converter units are able to limit the grid injected active power for upward ramps by forcing the PVG to work at lower power than the MPP [23]. This method, however, wastes energy and does nothing to limit downward ramps. What is essentially needed is a parallel active power compensating unit, similarly to reactive power compensation with a separate Static Var Compensator (SVC) or a Static Synchronous Compensator (STATCOM).

By utilizing an energy storage system both up- and downward ramps can be compensated by limiting them without wasting any energy. Figure 3.3 shows the basic principle of RR limiting implemented with a virtual ESS. The green grid feed-in power P_{grid} curve shows how the PVG power P_{PVG} should ramp up and down in order to comply with a RR limit of 10 %/min. Whenever the PVG power ramps exceed the limit, they are regulated with the assist of the ESS. Otherwise, the power fed into the grid follows the PVG power.

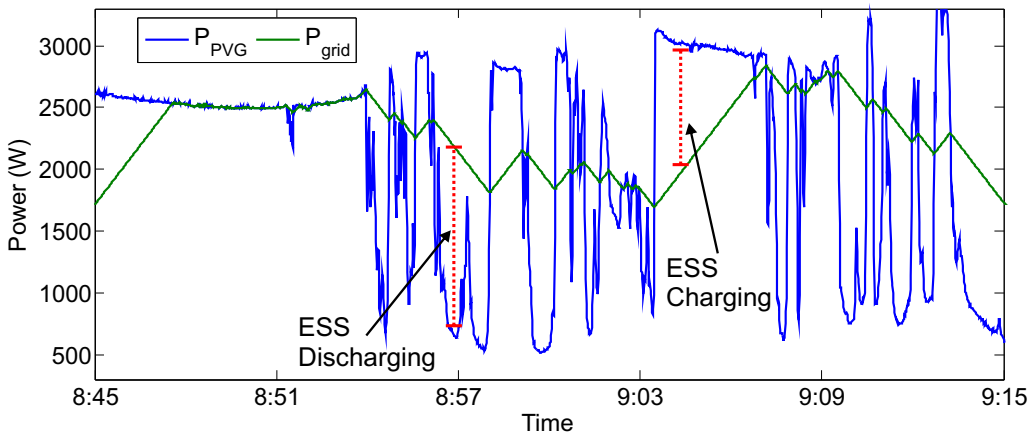

Figure 3.3. A sample of a 3.2 kWp PVG power evolution compared to an arbitrary 10 %/min ramp rate limit on 15.06.2015. The formation of momentary charge and discharge powers for a virtual energy storage system are highlighted with red bars.

Whenever downward ramps require limiting ($P_{\text{grid}} > P_{\text{PVG}}$) the ESS provides the additional energy to the grid, and whenever upward ramps require limiting ($P_{\text{grid}} < P_{\text{PVG}}$) the ESS stores the excess energy. Using a positive sign convention while considering the ESS as a supportive unit, the power fed into the grid is the sum of the PVG and ESS powers:

$$P_{grid}(t) = P_{PVG}(t) + P_{ESS}(t), \tag{3.2}$$

where $P_{\text{ESS}}(t)$ represents the momentary ESS power. The red bars in Fig. 3.3 depict how P_{ESS} support power is formed in respect to Eq. 3.2. Whenever the ESS provides energy it is discharged ($P_{\text{ESS}}(t) > 0$) and whenever it stores energy it is charged ($P_{\text{ESS}}(t) < 0$).

3.4.1 Energy Storage Technologies

The following section quickly reviews the possible ESS technology options and highlights the characteristics preferable in the fluctuation compensation application. Many ESS technologies exists today and they can be categorized in several ways, for instance by their storing mechanism:

- Electromagnetic: Super Magnetic Energy Storage (SMES), Super Capacitors
- Electrochemical: Li-ion, Lead, NaS, Ni-Cd, Flow, etc. batteries, Fuel cells
- Mechanical: Flywheels, Compressed Air Energy Storage (CAES), Pumped Hydro Storage (PHS)

Each of these technologies have their own characteristics which determine how well they perform in certain applications. Storage can be differentiated in attributes such as capacity, power rating, cycling durability, lifetime, efficiency, response rate, energy density, cost and maturity for instance.

The fast and frequent fluctuation behavior implies that the compensation application demands furthermost a storage that has a fast response rate and good cycling durability. Single energy release or storing events require relative low amounts of power and last from seconds to few minutes, therefore requiring only small or medium capacity and power capabilities from the storage. Characteristics such as low cost, high efficiency and high energy density are beneficial as well, but merely separate the plausible options further from each other. The required characteristics can also be case sensitive. For example, residential applications have system size constrictions that might rule out technologies with low volumetric energy density. Utility scale systems, however, might not suffer from the same issue. Table 3.1 shows key characteristics for some of the most considerable storage technologies. It should

be noted that the categories for Flow and Li-ion batteries include several different sub-technologies.

For the sake of comparison, Table 3.1 shows many different types of technologies, but it is evident from the figures that some of them are impractical in this application. Pumped hydro and compressed air storage systems are not responsive enough to suit the basic requirements. They also have great siting issues which can also be related to their very low energy densities. Super capacitors are still a developing technology with high costs, self-discharge rate and low energy density. The latter indicates that the system sizes of super capacitors in this application would be impractically large. However, they have been proposed to be used in parallel with other technologies to supply high power surges if necessary. Fuel cells and hydrogen technology have low efficiency, low lifetime and low cyclelife, which is especially problematic. The rest of the technologies in Table 3.1 are plausible solutions with their individual advantages and disadvantages. [24, 25].

Table 3.1. Key characteristics of some energy storage technologies. Boldface refers to the most favorable technology in each characteristic. Adapted from [25].

	Investment Cost (€/kWh)	Energy Density (kWh/m^3)	Lifetime (years)	Cyclelife (full cycles)	Round-trip Eff. (%)	Self-discharge (%/day)	Response Time
Pb-acid	50-300	75	3-15	2,000	80-90	0.1-0.3	ms
Li-ion	200-1,800	**250-620**	8-15	>4,000	**90-98**	0.1-0.3	ms
NiCd	200-1,000	<200	15-20	1,500	70-75	0.2-0.6	ms
NaS	200-900	<400	12-20	2,000 - 4,500	85-90	20	ms
Flow Bat.	150-1,000	20-800	5-30	2,000-13,000	60-75	0-10	**<ms**
Super Cap.	300-4,000	10-20	>20	**>50,0000**	85-98	2-40	ms
Hydrogen	**1-15**	600	5-15	>1000	29-49	0.5-2	ms-min
Flywheel	1,000-3,500	20-80	>20	10^5 - 10^7	85-95	20-100	ms-s
CAES	10-40	12	25-40	No lim.	<5	**0**	1-15 min
PHS	60-150	0.2-2	**50-100**	>5 x 10^12	75-85	**0**	s-min

Lithium-ion technology has many favorable characteristics in Table 3.1. It is responsive, has high efficiency and high energy density. Its lifetime is relative good and cyclelife can extend very high [26]. Its major disadvantages are high cost, relatively immature development phase, relatively small power rating and the necessity of support circuits. Nonetheless, its has advantages compared to other technologies which is why so many manufactures have chosen to use it in commercial renewable integration applications [26–31]. Other battery technologies, such as traditional lead-acid batteries, are also viable choices with slightly lower performance and costs compared to Li-ion. However, it should be noted that expensive Li-ion batteries with extended cyclelife can be economically more viable when considering the investment cost per cycle [31].

3.4.2 Enery Storage System Control Schemes

The ESS charge and discharge power can be found by working backwards from Eq. 3.2. The required amount of momentary P_{ESS} is calculated by applying a RR limiting scheme to a PVG power measurement. The limiting scheme can be realized with various different methods as long as the grid feed-in RRs satisfy the given limits. The green P_{grid} curve in Fig. 3.3 shows the maximum allowable rates of the power ramps, but it is also the output of the basic rule based RR limiting method. Rule based refers to the method forcing the output to follow a set rule:

$$[P_{\text{PVG}}(t-\Delta t) - \Delta t \cdot r] \leq P_{\text{grid}} \leq [P_{\text{PVG}}(t-\Delta t) + \Delta t \cdot r]. \tag{3.3}$$

Other methods of producing a limit compliant grid feed-in power exist as well. One well known method is the moving average method, which as it name implies, applies a moving average on the PVG power profile in order to smooth out rapid fluctuations. Another very similar method is the low-pass filtering method, which applies a filter instead of a moving average. Figure 3.4 depicts the behavior of these two limiting methods compared to the rule based rate limiter.

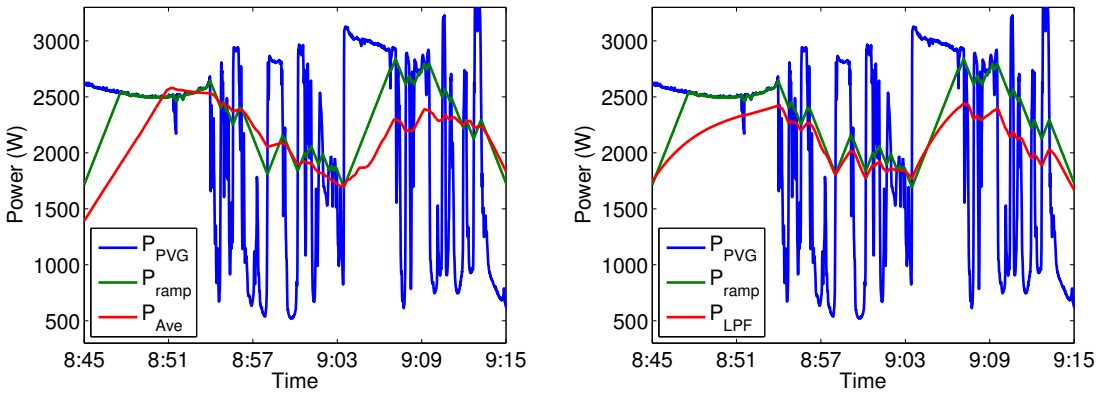

Figure 3.4. Ramp rate limiting with (a) moving averaging and (b) low-pass filtering compared to the rule based rate limiting. All limiters comply with a 10 %/min limit.

The moving average and low-pass filter methods shown in Fig. 3.4 produce smooth ramps that comply with the RR limit using different principles. Many studies have been made to compare the behavior and efficiency of these methods and most of them indicate that the basic rule based rate limiting is the most effective [32–34]. Other methods such as constant power or forecast reference have also been proposed as well. This thesis, however, focuses on studying ESS behavior only through the basic rule based rate limiting method.

3.4.3 Energy Storage System Interconnection

The ESS interconnection in this application can be realized in couple of different ways. Figure 3.5 shows two examples of typical connection topologies. Compared to traditional residential PV with battery storage systems the ESS requires more controllability. Thus the ESS is recommended to have a dedicated converter unit. The converter can be either a bidirectional DC/DC or DC/AC unit depending on whether the interconnection of the ESS and the PVG is done using a DC-bus like in Fig. 3.5a or an AC-bus like in Fig. 3.5b [13, 35]. Note that in Fig. 3.5b the PVG interfacing can also be two-staged if desired.

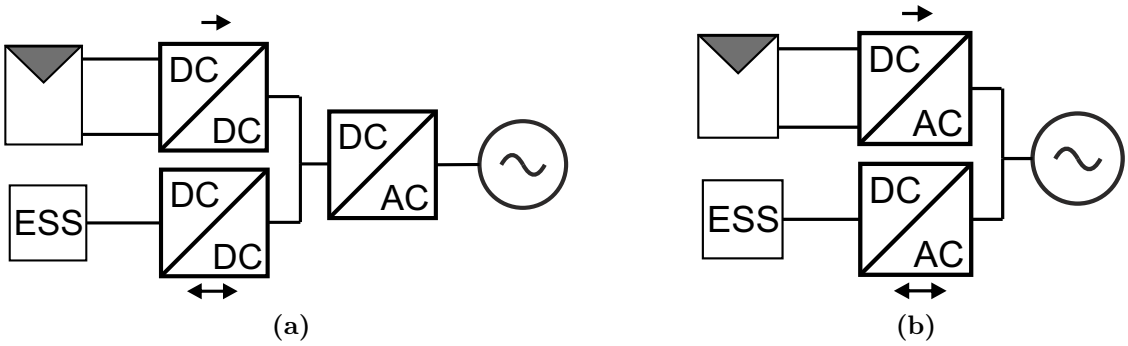

Figure 3.5. ESS and PVG interconnection topologies with (a) a DC-bus and (b) an AC-bus. The arrows in the figure depict the power flow directions.

An AC-bus is a likely choice in high power utility or commercial applications, and the DC-bus in low power residential applications. Both topologies are modular, meaning that the ESS and PVG can both have several units connected to the same bus. The ESS can even be a hybrid system of several different units realized with different storage technologies [36].

4. TUT RESEARCH PLANT AND MEASUREMENT DATA

The investigations and simulations presented in this thesis are based on the measurement system and data explained in this chapter. The data is obtained from the Solar PV Power Station Research Plant of Tampere University of Technology [9]. The plant contains six different PV string combinations consisting of 69 NAPS NP190GKg PV modules mounted on the planar roof of the Sähkötalo cambus building. All modules are facing southwards and tilted 45° from the roof plane. The strings are embedded with a network of 24 irradiance and temperature sensor pairs. Figure 4.1 shows the layout of both the plant and the sensor network. The plant is located approximately at 61°27'04.7"N and 23°51'27.1"E.

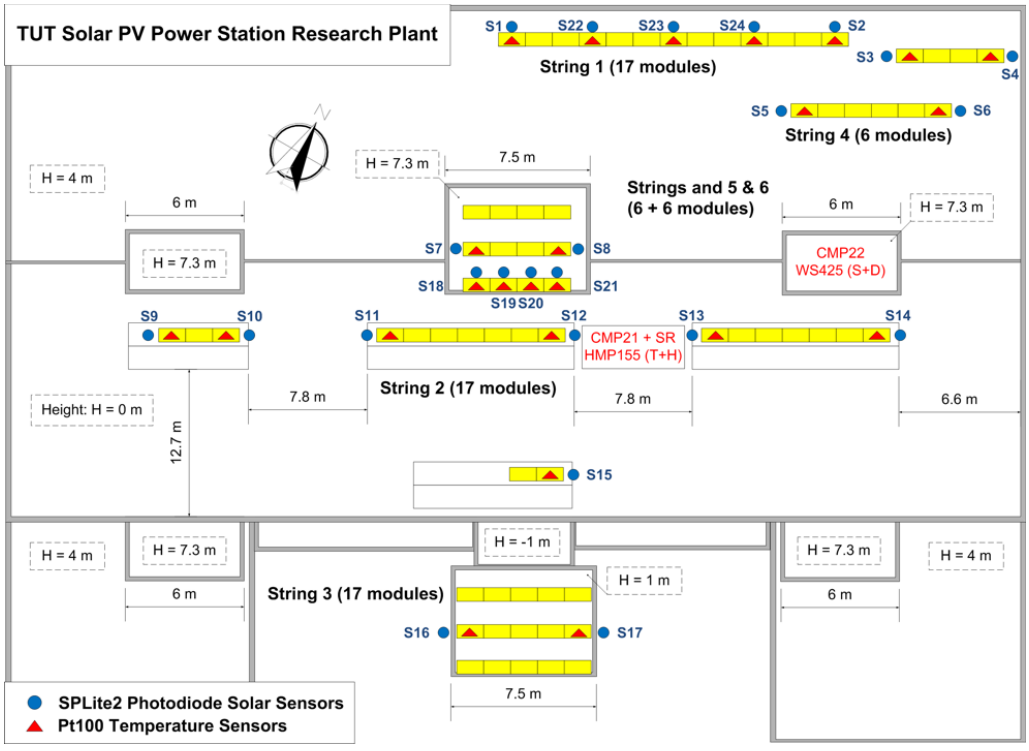

Figure 4.1. General layout of the TUT solar power plant and its sensor network [9].

The irradiance sensors are photodiode based SP Lite2 pyranometers manufactured by Kipp & Zonen. They are Plane of Array (PoA) sensors that are mounted next to selected PV modules with the same 45° tilt angle. The temperature sensors

are PT100-type thermal sensors mounted to the backplates of the selected modules. Atmospheric temperature, wind, humidity and global and diffuse irradiance measurements are also available. All measurements are synchronized and measured with a 0.1 Hz frequency. The plant has been operating since 2011 collecting comprehensive data for more than three consecutive years. The outermost sensors surround an unevenly shaped area of 2,300 m^2.

Additionally module and string powers can be measured with a self-designed IV-curve tracer. The tracer uses series-connected IGBT-switches that are simultaneously switched open to drive the PVG from open to short-circuit while the voltage and current during the transition are measured with a 100 kHz frequency. The tracer enables the examination of the electrical behaviour without the influence of interfacing devices. In this thesis the IV-data is used to detect the momentary maximum power of PVGs.

All the data used for the analyses of this thesis was scaled to 1 Hz sampling frequency. In order to filter out measurement noise all measurements were evened with a 5 second moving average. Specific sensors were selected for each examination based on their location and consistency of measurements. This way best possible accuracy and reliability are guaranteed.

5. PV POWER MODELLING

The most straight-forward way to study PV power fluctuations would be to investigate power data. However, examining power data would limit the study to the specifications of the generator the data was obtained from. A more generally applicable method is necessary in order to derive more generic conclusions. Due to the direct proportionality between PV power and incident irradiance shown in Ch. 2.2, irradiance data can be used to model PV power without being constricted to a specific PV plant and its behavior. This chapter examines the various factors affecting the variability of PV power and its modelling.

5.1 Spatial Smoothing of Irradiance Variability

Irradiance is the main factor in PV output modelling due to the strong dependency between these two variables. However, PV power is approximately proportional to a spatial irradiance profile rather than a single sensor measurement [15–18]. The concept of spatial irradiance G_{s} is used to represent the irradiance of an area A with multiple different irradiance conditions locally. Fast ramps of local irradiance variations tend to smooth out in the spatial irradiance. This phenomenon is called spatial smoothing, and its effect increases with increasing area [15, 37, 38].

Technically, measurements from a single sensor represents only the irradiance of the very small area the sensor eye covers, hence it is called a point measurement. As the distance between multiple point sensors is increased, their readings begin to differ because local irradiance conditions differ from each other. Like mentioned in Ch. 3 PV variability is a function of timescale, and the shorter the timescale the bigger the differences between local variability. Combining the effect of several synchronized sensor readings into one spatial irradiance profile filters out the short timescale fluctuations and smooths the ramps of steep fluctuations. Figure 5.1 demonstrates the concept of the smoothing effect.

PVG output power behaves approximately the same way as spatial irradiance, regardless of the generator topology. Intuition says that if the power of a single PV module is proportional to its incident irradiance, then the combination of several dispersed modules follows the combination of several local irradiance conditions. Yet another way to examine this, is to understand that technically a large PVG is an irradiance sensor with a large surface. Its output is the aggregate of irradiance

hitting its dispersed subsections.

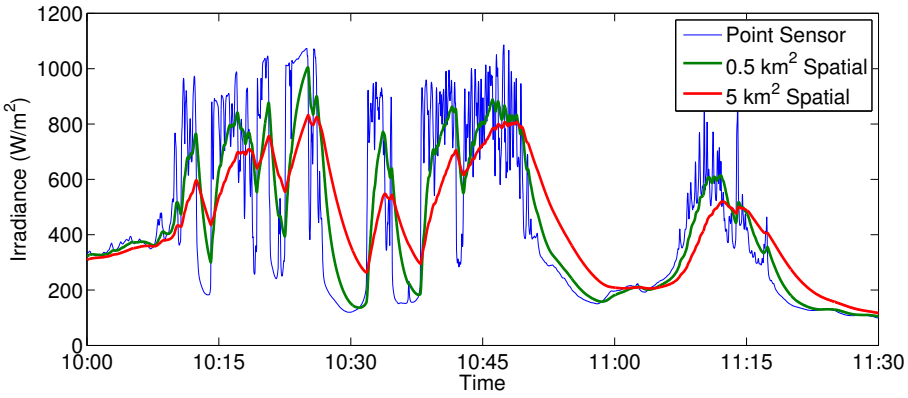

Figure 5.1. Concept of spatial smoothing of an arbitrary irradiance profile from point sensor measurement to a 0.5 and 5 km^2 square areas. Point sensor measurement obtained from sensor S12 on 13.7.2012.

In [37] the extend of spatial smoothing was determined by comparing the ramp correlation of point sensor pairs with various distances starting from 90 m. The results indicate that the minimum threshold of significant smoothing is somewhere between 90 m and 450 m. Similar results with a slightly different approach were obtained in [38]. These results indicate that a rectangular PVG area with the shortest side of approximately 100 m or under will experience marginal spatial smoothing. As a notion, this applies to the TUT plant ($A = 2,300$ m^2) and all the strings inside it.

5.1.1 Spatial Irradiance Modelling Techniques

Depending on the size of the PVG, it is far more accurate to use a model of the spatial irradiance rather than a point sensor measurement to approximate PV power. Several ways of modelling spatial irradiance exists. Most modelling methods aim to smooth out point measurements in various ways. The most applicable methods require the least amount of computation and input data.

A simple method is to average several synchronized point sensor measurements [17,39–42]. In order for the aggregate to be spatially balanced the sensors should be evenly spaced and surround a specific area. The denser the sensor grid is, the more accurate the aggregate becomes. Theoretically a perfect spatial aggregate could be obtained with a sensor representing each individual PV module. The clear drawback of this method is the high cost of the large amount of sensors.

Another simple method is to time average a single point measurement with a moving average [43]. The averaging window is based on the time it takes for a cloud to pass over a square PVG area. It can be calculated with $t = \sqrt{A}/v_c$, where A is

the PVG area and v_c is the cloud speed. The cloud speed can be either indirectly measured or modelled. Using a dynamic v_c makes the model more accurate since it alters the amount of smoothing based on cloud movement. Obtaining a reliable measure for the cloud speed makes this method difficult to implement.

A third method proposed in [44] is to smooth a point measurement with a low pass filter. The Fourier spectra of a point sensor measurement and a PVG power match at low frequencies (long timescales). The PVG power spectra has also a plant area dependent frequency, at which the power variability starts to attenuate increasingly. Several power measurements from Spanish PV plants were used to experimentally verify that the same frequencies could be used as the cut-off frequency of a filter. The filter could be applied to irradiance point measurements to produce spatial irradiance profiles, that fitted well to power measurements. The continuous transfer function for the filter in Laplace-domain can be expressed with:

$$\frac{G_{\mathrm{s}}(t)}{G(t)} = \frac{1}{(\frac{\sqrt{A}}{2\pi \cdot 0.02})s + 1}, \tag{5.1}$$

where G_{s} is the spatial irradiance, G the irradiance sensor measurement, A the spatial area in hectares and s the Laplace-variable. The coefficient 0.02 is an experimentally verified number. For a more descriptive representation $\sqrt{A}$ can be substituted with $d/100$, where d is the PVG square area dimension in meters. This method is simple, validated to produce good results and requires only one point measurement. The method assumes a square PVG area, however. The authors of [44] do not touch the subject of modelling other than square areas. Thus, it falls to the user to determine an equivalent square area if other area shapes are to be modelled.

One acclaimed method is the Wavelet Variability Model (WVM) [45]. It utilizes the idea of different spatial irradiance smoothing at different timescales. In VWM a wavelet transform is used to divide an irradiance point measurement into different timescales, after which variance in each timescale is reduced by a timescale dependent amount. The amount of reduction is determined from daily variability correlation between various sensor pairs at different distances and timescales. This way the method can take into account the plant area, the effect of cloud speed and also the module density. Although the method has been verified to be accurate, it is quite complicated. It requires clear sky modelling, processing of 12 different timescales and either cloud speed data or several point sensor measurements.

5.2 Other Modelling Factors

Other factors affecting the output of PVGs are less prominent than irradiance, but effective nonetheless. Taking these factors into account yields additional accuracy.

Sources of shading or reflection, such as soiling, snow, buildings or water can alter the amount of irradiance on the modules [10]. The effect of these factors can have long durations but also change quickly. For example a pile of snow can cover a module for a long period but slide off quickly in the right conditions. Usually these effects are small and can be modelled with a constant reduction or addition to the power output. Assuming that a plant is correctly designed, installed and maintained these factors can even be overlooked withouth loosing much accuracy.

As was mentioned in Ch. 2 module temperature has significant effect to the generator power. Thus, it is the biggest factor after irradiance to affect PV variability modelling. The temperature dependency of PV cell efficiency depends on the cell technology. The maximum power of a typical crystalline silicon cell decreases approximately 0.5 %/°C [10] as was show in Ch. 2.2. Module temperatures usually create offset to PV power expectations that are based on nominal values or STC conditions. Accurate PV output modelling requires either module temperature measurements or a dynamic temperature model. Temperature models are usually based on the incident irradiance and ambient condition measurements. When high accuracy is required while considering large and dispersed PVGs, spatial temperature differences should also be taken into account similarly to spatial irradiance. However, the findings reported in [46] indicate that the largest module temperature difference in both close proximity and highly dispersed PV modules is only about 6-7 °C.

PVG power is also affected by mismatch losses [10]. When several PV modules are series connected into a string they have the same current travelling though all modules. If the operating conditions of the modules are even slightly different, the modules with lower current production can either hinder the string current or be bypassed with diodes. If a string does not extent to very long distances or have long spacing between modules, then the modules share similar conditions and these losses are relatively small. Detailed dynamic models such as the one-diode-model can be used to take these losses into account. [10]

The power electronic converters used in PV systems produce losses as well. The varying efficiencies of these converters depend on the operating conditions, but peak efficiencies are generally higher than 95 %. Another loss associated with these converters is their peak output power limit. Even if a PVG could exceed its nominal power its converter will not be able to produce more power than it is rated for. Since these converters control the PVG operating point they are also responsible for any possible MPP tracking losses. These losses depend on the type of the tracking algorithm and its tracking delay. Perturbing MPPT algorithms will also cause additional small scale fluctuations in the PVG power. Detailed converter models exist for simulating all of these factors. [12, 13, 47]

Additional losses can be caused by transmission lines and transformers. Usually these losses are assumed to be relatively constant and modelled with constant multipliers.

5.3 Chosen Modelling Method

In this thesis a specific PV power modelling method is used. All considerations and the validation of the method are presented in this chapter. In order to produce an accurate study the resolution of examined time series needs to be high. High resolution of 1 s guarantees that even very short and fast fluctuations are registers. Additionally, a long study period extending over a full year is required, since all the possible seasonal conditions need to be included and all phenomena should have clear periodicity. These requirements lead to time series with more than 31 million data points per each measurement. In order to be able to compute such a large amount of data, the modelling method needs to be simple. Therefore, out of all the modelling options reviewed in the previous chapters, only the most crucial factors, spatial smoothing and temperature effect, are implemented using the simplest methods.

The model is simplified and generalized by assuming some idealities. Soiling, reflections, mismatch losses, converter losses, MPPT losses, transmission and transformer losses are all neglected. Some of these losses, mainly mismatch and converter losses, also require specifying a PVG technology, which goes besides the point of a generally applicable model. Hence the model will slightly overestimate the power but remain generic. The use of arbitrary but ideal converters are assumed in most of the upcoming examinations. The converters are assumed to be sized based on the generator nominal power $P_{\mathrm{PVG,nom}}$ and not capable of producing more power than what they are rated for. Thus, the output of the model is limited to $P_{\mathrm{PVG,nom}}$.

The low pass filter method of Eq. 5.1 is used for modelling spatial smoothing. It is selected because it is easy to compute and requires only the plant area and a single point measurement as inputs. Note, that before it can be used with a discrete time series the transfer function in Eq. 5.1 has to be discretized. Appendix A describes the discretization process.

The effect of module temperature T is implemented into the power model as an approximate 0.5 % addition or reduction to power for each degree that deviates from STC conditions:

$$P_{\mathrm{mod}}(t) = \frac{P_{\mathrm{PVG,nom}}}{G_{\mathrm{STC}}} \cdot G_{\mathrm{s}}(t) \cdot [1 - 0.005 \frac{1}{^{\mathrm{o}}\mathrm{C}} \cdot (T(t) - T_{STC})], \tag{5.2}$$

where G_{STC} is the STC irradiance, G_{s} the spatial irradiance input obtained with Eq. 5.1 and T_{STC} the STC temperature. In this thesis the module temperatures are obtained from backplate temperature sensors of the sensor network shown in Ch. 4.

5.3.1 Model Validation

The accuracy of the model's power approximation was validated with a comparison to actual PVG power measurements obtained with the IV-curve tracer. Before going into the comparison, a noteworthy observation of the spatial smoothing should be outlined. Due to the very small area of even the largest TUT plant PV strings, any spatial smoothing is insignificantly small, as was concluded at the end of Ch. 5.1. Therefore, the use of the spatial irradiance modelling is not necessary with the very small PVGs used in the follow-up verifications. Unfortunately this means that the model cannot be fully validated. Nonetheless, the results shown in [44] are convincing enough to satisfy the needs of this thesis.

To begin with, eight hours of measurements from string 1 ($P_{\mathrm{PVG,nom}} = 3.2$ kWp) on 20.04.2015 were studied. An irradiance point measurement (S2) from the vicinity of string 1 was compared to the string maximum power evolution, while the back-plate temperature measurement (S2) was also monitored. The results are shown in Figure 5.2. To allow a proper comparison G plots are normalized to STC irradiance and P to nominal power.

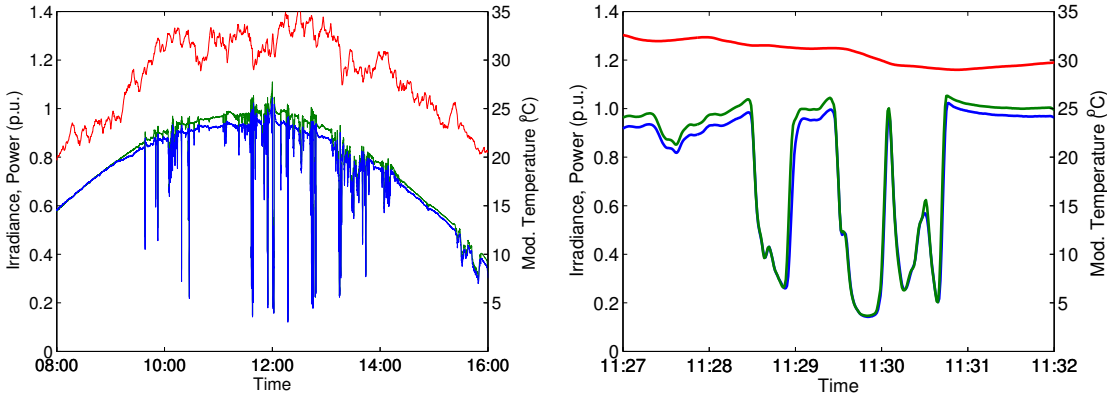

Figure 5.2. Measured string 1 power (blue), sensor S2 irradiance (green) and module temperature (red) on 20.04.2015 from (a) 8 AM to 4 PM and (b) a 5 minute sample from midday.

Fig. 5.2 shows how the transitions of measured P and G correlate well, but there is a clear offset at midday. The offset is caused by the high module temperature which lowers the maximum power. The difference clearly increases as the temperature accumulates towards midday, and decreases when the temperature starts to fall in the afternoon. If ESS usage would be simulated based on this G measurement, the power and capacity requirements of the ESS would be overestimated by the amount of the offset. Thus, this offset needs to be mitigated by using the power model, which has the module temperature taken into account with Eq. 5.2. Figure

5.3 shows a comparison of the power measurement, irradiance measurement and modelled power. In the figure the modelled and measured power plots align well and the offset has been clearly reduced.

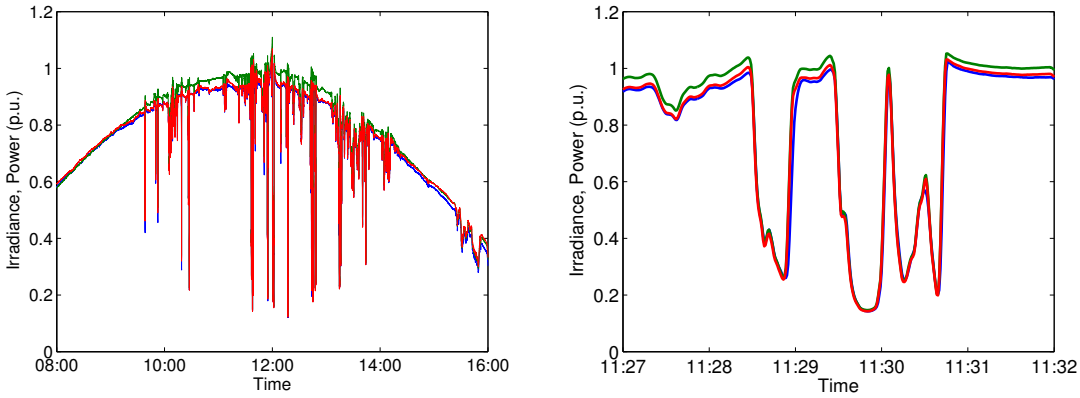

(a) **(b)**

Figure 5.3. Measured string 1 power (blue), sensor S2 irradiance (green) and modelled power (red) on 20.04.2015 from (a) 8 AM to 4 PM and (b) a 5 minute sample from midday.

Figure 5.4 shows another example where the model conforms with the measured power when the module temperature decreases. When the module temperature is high the irradiance has a higher value than the measured power, but the situation is reversed when the module temperature drops. The modelled power accurately follows the measured power in this situation.

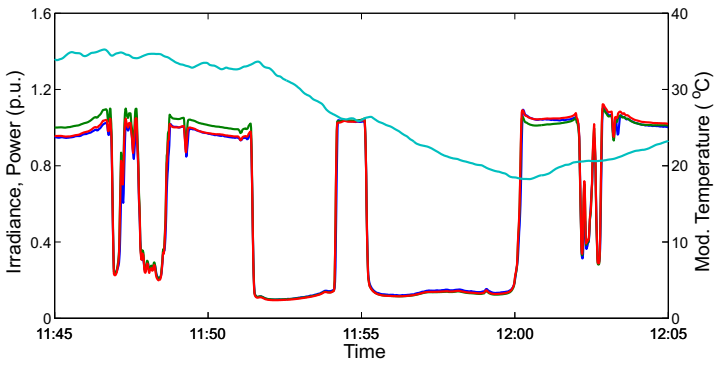

Figure 5.4. String 2 power (blue), spatial irradiance (green), modelled power (red) and module backplate temperature (turquoise) on 13.04.2015.

The examination was done for 30 days using Strings 1, 2 (both $P_{\mathrm{PVG,nom}} = 3.2$ kWp) and 4 ($P_{\mathrm{PVG,nom}} = 1.14$ kWp). The majority of these days were recorded from the middle of April, May, June and July 2015, while the rest of the data was recorded in July 2013. All days contain 8-14 hours worth of data from around midday. The

selected days contain overcast, clear sky and partially cloudy days with both high and low ambient temperatures to cover a diverse set of conditions. Visual inspection of each day shows a good fit for the simulated and measured powers. On days with low irradiance the modelled power can be slightly overestimated and deviate more from the power than the irradiance measurement. Nonetheless, these issues are marginally small compared to the added accuracy in other conditions.

The method was also validated statistically in two different manners. Since the area of interest in this thesis are ramp rates, the model should produce them as accurate as possible. Thus, a method used in [44] was adapted to verify the differences between the daily extreme RRs of the modelled and measured powers with:

$$D = (\frac{|\Delta P_{\text{meas}}|}{P_{\text{nom}}})_{\max} - (\frac{|\Delta P_{\text{mod}}|}{P_{\text{nom}}})_{\max}, \tag{5.3}$$

where ΔP is calculated with Eq. 3.1. The accuracy of the model can be determined by repeating the said calculation for the daily irradiance measurements respectively and comparing the results. Additionally, the daily Root Mean Square Differences (RMSD) to the measured power were calculated for the modelled power and the irradiance measurement and compared to each other.

The comparisons reveal how most of the time both the model and irradiance overestimate the ramp rates by 0-4 %. However, only on seven days the model predicts the extreme RRs less accurately than the irradiance measurement. Similarly the model has a larger RMSD than the irradiance only on seven days. Table 5.1 shows the collected mean and Standard Deviation (STD) of the D and RMSD values from the 30 days.

Table 5.1. Mean and STD of daily extreme RR and RMSD for modelled PVG power and irradiance measurement compared to real PVG power measurements during 30 selected days.

	D_P	D_G	RMSD_P	RMSD_G
Mean (%)	-0.77	-1.36	2.00	3.26
STD (%)	0.78	0.93	0.92	2.07

The results of table 5.1 show how the figures are very small in all cases, but the simulated power is statistically slightly more accurate. These results indicate that the presented method has a small error in approximating PVG power and that using the temperature correction creates more accuracy for the model.

It should also be noted that the above examinations used a 1 second timescale. Longer timescales are expected to show more deviation between the model and the measurement. However, this issue does not concern this thesis because all examinations are done in the one second timescale.

6. BEHAVIOUR, CONTROL AND SIZING OF THE ENERGY STORAGE SYSTEM

In this chapter simulations of virtual PV generators with arbitrary storage systems are studied in order to analyse the system behaviour and derive ESS sizing guidelines. The biggest factors of interest are the ESS power and capacity requirements and the stress withstanding capabilities.

The simulated PVGs use the power model presented in Ch. 5 with measurements from sensors S12 measured during the leap year 2012. These sensors have a central location and consistent measurements for the selected year. Out of 366 days the data has 17 days with insufficient data (30 minutes or more missing). These days are overlooked which leaves 349 days (95 %) for examination.

The virtual ESS is assumed to be an ideal storage of undefined technology, capacity, power rating and connection to the PVG. Leaving these factors undefined allows the examination of the requirements that the PVG application defines. The required momentary ESS power can be calculated with:

$$P_{ESS}(t) = P_{\text{grid}}(t) - P_{\text{PVG}}(t), \tag{6.1}$$

This form follows the convention defined in Ch. 3. Implementing the ramp rate control to a discreet P_{grid} time series can be done with a simple rate limiter algorithm:

$$P_{\text{grid}}(t) = \begin{cases} P_{\text{grid}}(t-\Delta t) + r\Delta t\ , & \text{if } P_{\text{PVG}}(t) - P_{\text{grid}}(t-\Delta t) > r\Delta t \\ P_{\text{grid}}(t-\Delta t) - r\Delta t\ , & \text{if } P_{\text{PVG}}(t) - P_{\text{grid}}(t-\Delta t) < -r\Delta t\ , \\ P_{\text{PVG}}(t)\ , & \text{else} \end{cases} \tag{6.2}$$

where t represents the current time step and $t-\Delta t$ the previous time step, r is the ramp rate limit and Δt the sampling time. Although r is usually expressed with %/min in Eq. 6.2 the proper unit is W/s. The momentary ESS energy is calculated as a discrete integral of the ESS power:

$$E_{\text{ESS}}(t) = E_{\text{ESS}}(t-\Delta t) - ([(P_{\text{ESS}}(t) + P_{\text{ESS}}(t-\Delta t)] \cdot \frac{\Delta t}{2}). \tag{6.3}$$

6.1 Short Timescale Behaviour

Let us start by examining simulation results of a 1 kWp virtual PVG equipped with the arbitrary ESS. The ramp rate limit was set to an arbitrary value of 10 %/min (1.67 W/s). First the short timescale behaviour was examined. Figure 6.1 shows an isolated one hour sample of the simulation results during a half cloudy summer day with a lot of fluctuations.

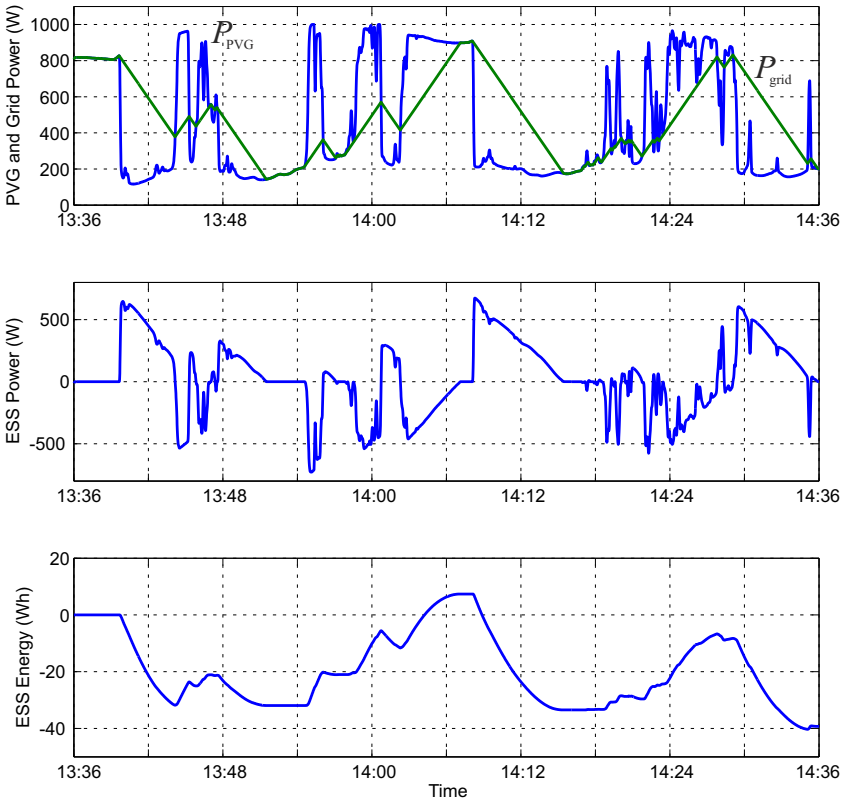

Figure 6.1. PVG power (blue), grid power (green) and the resulting ESS power and energy development from a one hour ESS simulation at midday on 27.07.2012.

One of the most interesting factors are the extreme power peaks, which give a good starting reference for determining the ESS power rating. The middle plot in Fig. 6.1 shows a typical sub-hourly behaviour of the highly fluctuation P_{ESS}. Power peaks are formed at the beginning of very large P_{PVG} fluctuations, where the PVG power changes very rapidly while P_{grid} steadily obeys the limit. As the difference between the two power variables gradually diminishes, P_{ESS} slopes to 0 W. In Fig. 6.1 P_{ESS} peaks range from approximately ±700 W. However, the whole year should be examined before drawing any conclusions on the required ESS power rating.

Another interesting observation is the maximum ramp rate of P_{ESS}, which determines the required ESS response rate. The fastest one second P_{ESS} ramp recorded in Fig. 6.1 is 121 W/s and the largest ramp from 0 to 670 W happens in 11 seconds. The ESS has to be able to also reverse the direction of its power flow instantly. From these indications it is quite evident that the ESS needs to utilize a technology capable of responding immediately, e.g. flywheels or batteries.

Now let us look at the energy development of the ESS shown in the lowest plot in Fig. 6.1. At 0 Wh the energy is in balance, negative energy refers to energy deficiency caused by discharging and positive energy to energy surplus caused by charging. The minimum capacity of the ESS can be defined as the difference between the maximum and minimum energy values cycled in the ESS:

$$C_{\mathrm{ESS}} = E_{\mathrm{ESS,max}} - E_{\mathrm{ESS,min}}. \tag{6.4}$$

The energy deficiency and surplus accumulate by a rate defined by the amplitude and duration of P_{ESS} evolution. The biggest accumulations are experienced when a large P_{PVG} fluctuation causes a steady and uninterrupted P_{grid} ramp. However, the complex development of unequal charge and discharge cycles requires the minimum and maximum value examination from a longer period.

6.2 Energy Development in Longer Periods

Let us examine the evolution of E_{ESS} in longer periods. At first it may sound like the back and forth nature of PV fluctuations would naturally keep the energy balanced to 0 Wh. This is the case in periods from minutes to couple of days, but eventually in several days the energy deficiency tends to accumulate so much that it is unlikely to be fully balanced to 0 Wh by a series of charges. Figure 6.2 shows E_{ESS} development from a simulations of a single day and 30 summer days. The accumulation of energy deficiency is evident in both periods. Extending the simulation to a full year would show exactly the same behaviour. If the PVG power is curtailed and the excess energy is utilized in the ESS, the evolution could also accumulate surplus because of the additional charging chances. However, the effect of curtailment is not examined in this thesis.

The accumulated energy deficiency clearly necessitates that the storage has to be forcefully charged at some point to counter the deficiency. The frequency of this forced charge has a major impact on the ESS capacity. For example in Fig. 6.2b the capacity would be defined mostly by the accumulated energy deficiency reached close to the end of the 30 day period. If similar behaviour is assumed to be expected every month and the storage is charged every 30 days, then the required capacity is approximately 800 Wh. Alternatively, if the charging period is reduced to the single

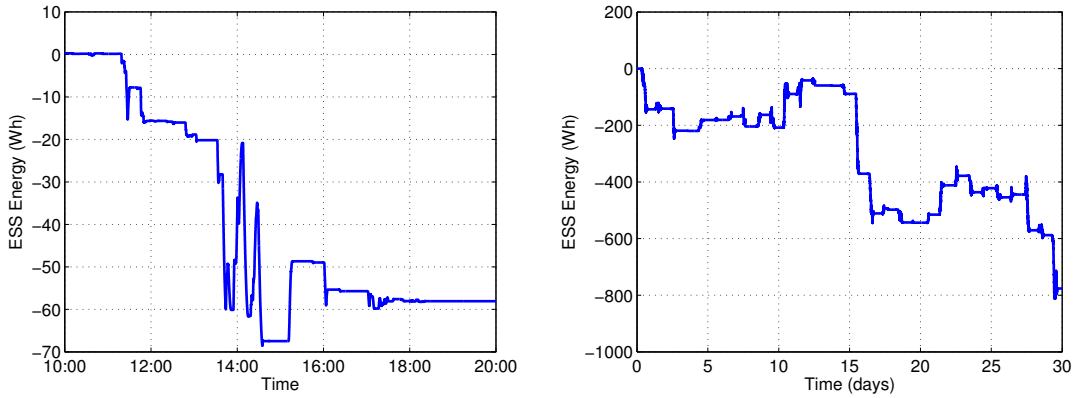

(a) **(b)**

Figure 6.2. ESS energy evolution during (a) 27.07.2012 and (b) 4.7.-3.8.2012.

day case of Fig. 6.2a the capacity requirement is only 70 Wh. Charging at shorter intervals can clearly lower the requirement. Therefore, the capacity can be heavily minimized through frequent forced charging.

6.3 State of Charge Control

A more sophisticated energy balancing method that develops the forced charge idea further is the State of Charge (SoC) control. It is a control method that actively charges and discharges the storage in order to keep the energy balanced at a specific reference level $E_{\mathrm{ESS,ref}}$. It works constantly by discharging excess energy to the grid and charging deficient energy from the PVG even when ramp rate limiting is not momentarily required. SoC control is especially valuable in battery applications, where it prolongs battery life by promoting partial charge cycles over full cycles resulting in less stress and degradation [48, 49].

A block diagram in Figure 6.3 displays the SoC control principle implemented into the ramp rate control. The $E_{\mathrm{ESS,ref}}$ is the reference energy state that the controller tries to keep in the storage. In most cases this reference is set to half of the effective storage capacity, since the ESS is charged and discharge in random order. The loop with the K parameter represent the SoC control. It uses a simple P-type controller that requests K times the E_{error} amount of power P_{SoC} for charging or discharging the ESS. By adjusting P_{SoC} through K and $E_{\mathrm{ESS,ref}}$ the speed of the SoC control can be adjusted. The difference of P_{PVG} and P_{SoC} is the input of the ramp rate limiter, thus, the difference also substitutes P_{PVG} in Eq. 6.2.

Figure 6.4 displays examples on how SoC control alters the amount of energy cycled through the storage. The energy reference was set to 0 Wh, r to 10 %/min and K to $5 \cdot 10^{-4}$. Fig. 6.4a shows how the control works to balance the energy level. The energy or its deficiency may accumulate with consecutive fluctuations, but once

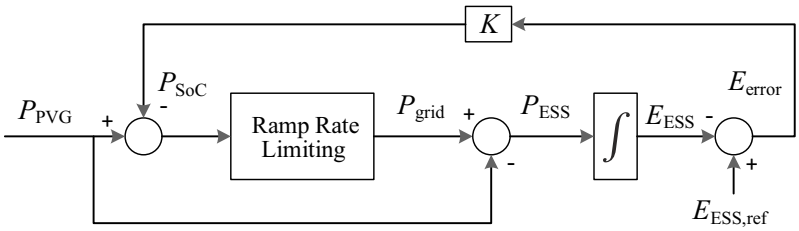

Figure 6.3. Control block diagram for PVG ramp rate control with state of charge balancing. Adapted from [50].

the fluctuations end the energy is slowly balanced towards the reference value. The same thing happens towards the end of the day, when all variability ceases and the control has an opportunity to balance E_{ESS} during the evening.

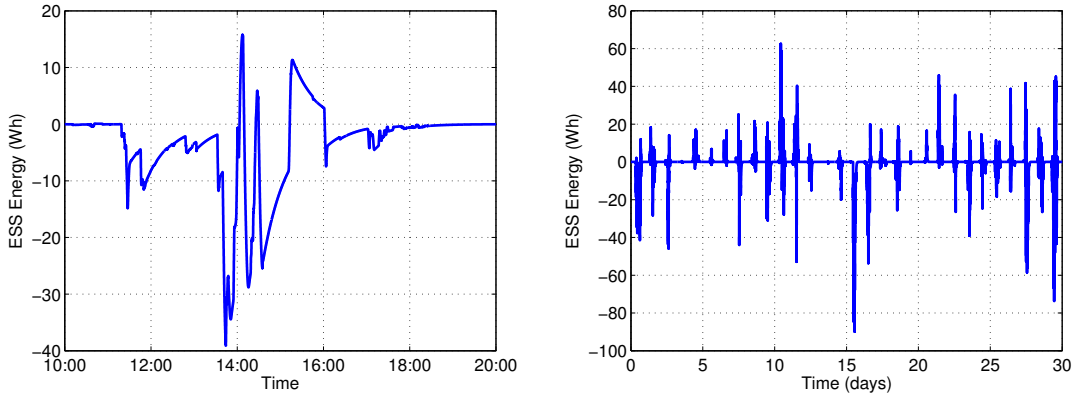

Figure 6.4. ESS energy evolution with SoC control during (a) 27.07.2012 and (b) 4.7.-3.8.2012.

Fig. 6.4 displays the same days as in Fig. 6.2 but with notably smaller extreme values due of the SoC control. By utilizing SoC control the capacity was reduced from 70 to 55 Wh for the one day period in Fig. 6.4a and from 800 to 155 Wh for the 30 day period in 6.4b.

6.3.1 State of Charge Control Behaviour and Optimizing

SoC control greatly alters the grid feed-in behaviour of the system. Figure 6.5 shows the P_{grid} evolution during the same isolated midday case as in Fig. 6.1 using SoC with two different K values and a 10 %/min RR limit. The figure shows how the SoC has a tendency to create difference between P_{grid} and P_{PVG} in order to quickly balance the ESS energy to its reference. The further away from the reference E_{ESS} is, the larger the momentary balancing power request is. Thus, the difference between PVG and grid feed-in powers is also larger. Fig. 6.5 also shows how the parameter

K can further influence this behaviour. Ultimately, the RR limit also influences this behaviour. Stricter limits require more energy from the ESS and thus their balancing require more power or time.

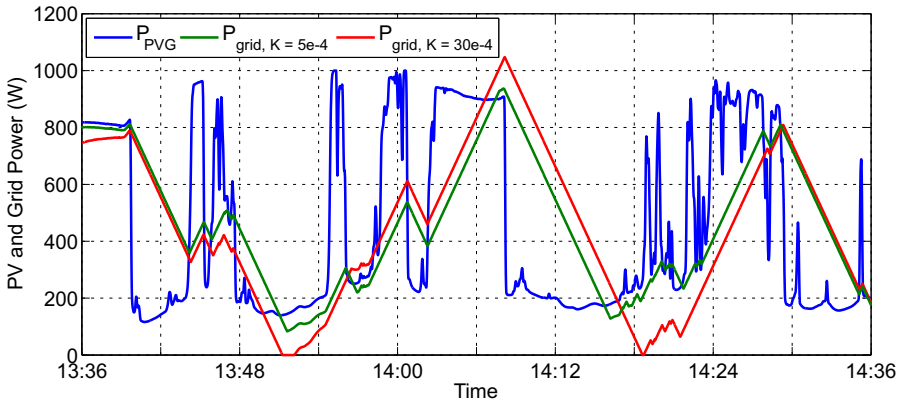

Figure 6.5. PVG and grid feed-in power evolution using SoC control with two different K parameter values at midday on 27.07.2012.

The main purpose of adjusting K is to adjust the speed of the ESS energy balancing. Figure 6.6 displays how a larger K value speeds up the energy balancing in a simple P_{PVG} step change simulation. Using too moderate K values will result in very slow energy balancing, while using too high values will cause instability to P_{grid}. For best results K should be optimized for individual situations. Thus, in some cases a dynamic K could serve better than a constant one. When using a constant K value some compromising between SoC speed and grid feed-in stability might be necessary. A recommendable K range has been experimentally verified to be approximately from $5 \cdot 10^{-4}$ to $20 \cdot 10^{-4}$.

As Fig. 6.5 shows, after large fluctuations the SoC control can drive the grid feed-in power beyond the momentary PVG power levels in both up- and downward ramps. Some upward ramps may overshoot beyond the PVG nominal power limits. It is recommended for P_{grid} to have an upper limit based on the PVG nominal power to take into account possible overloading of the feeder transformer. Such transformers can be assumed to be sized based on the nominal PVG power and thus the ESS and the behaviour it promotes should comply with it as well. Likewise, some downward ramps can undershoot P_{PVG} even enough to go below 0 W (at 13:49 in Fig. 6.5 with $K = 30 \cdot 10^{-4}$). Naturally a power generating unit is assumed to deny such requests and thus the lower P_{grid} limit is set to 0 W. Issuing such limits will result in some P_{grid} ramps to saturate to them. Saturation to the upper limit proposes no real problem but saturation to 0 W is a production outage which is a clear problem.

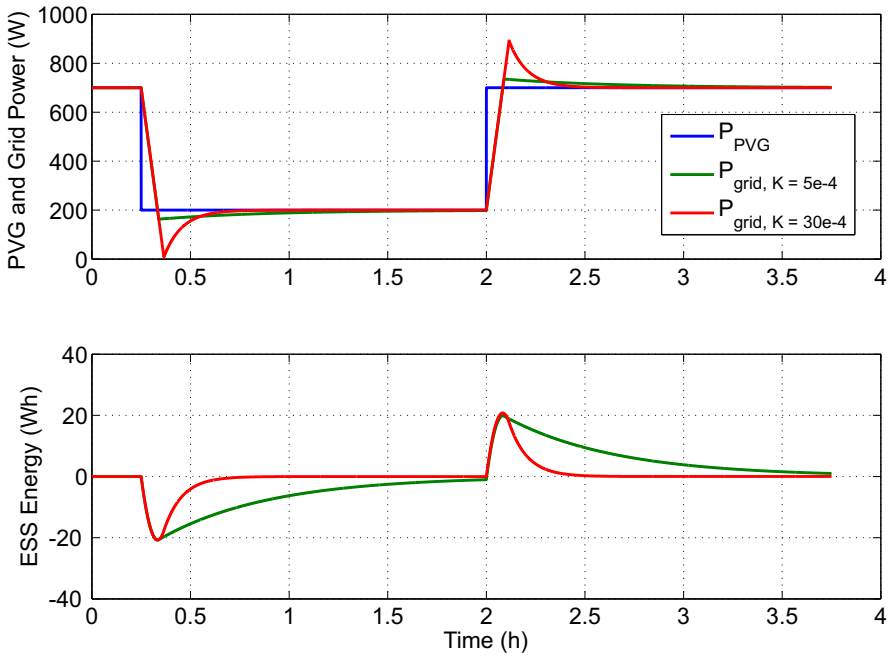

Figure 6.6. PVG and grid feed-in power and ESS energy response in a PVG power step change test using SoC control with two different K parameter values.

6.3.2 Proposed Solutions for the Production Outage Problem

The purpose of the ESS is to reduce grid feed-in instability issues, not to cause them by adding power production outages. To increase P_{grid} stability while utilizing SoC control the system requires additional control regulation. In this section two methods for production outage minimization are proposed. Both methods aim to achieve more P_{grid} stability without additional ESS sizing requirements compared to the regular SoC control (henceforth referred to as Method 0).

The first proposed method (Method 1) is based on regulating P_{SoC} whenever it proposes a problem. The amount of the P_{SoC} after downward ramps can be more than the low level of P_{PVG} can support, resulting in production outages. The problem can be mitigated by regulating P_{SoC} with the following logic:

- $P_{\text{SoC}}(t)$ is limited to a selected proportion of its value. A 10 % proportion is recommended
- Regulation starts to apply when $P_{\text{grid}}(t) < P_{\text{PVG}}(t)$ and $P_{\text{SoC}}(t) \leq 0.9 \cdot P_{\text{PVG}}(t)$
- The regulation is removed when ESS energy meets its reference, in order to avoid disturbance due to rabidly changing conditions

Figure 6.7a shows how the grid feed-in of this method compares to regular SoC control. In the figure Method 1 limits the maximum difference between P_{grid} and

P_{PVG} and thus prevents an outage. As Figure 6.7c shows it slows down the ESS energy balancing but only when it is necessary in order to avoid an outage. Unfortunately this method cannot guarantee that production outages are avoided in all cases. The limiting of P_{grid} is proportional to P_{SoC}. If P_{PVG} ramps very low, even a small proportion of P_{SoC} can be momentarily greater than P_{PVG}. In this situation P_{grid} can go to 0 W.

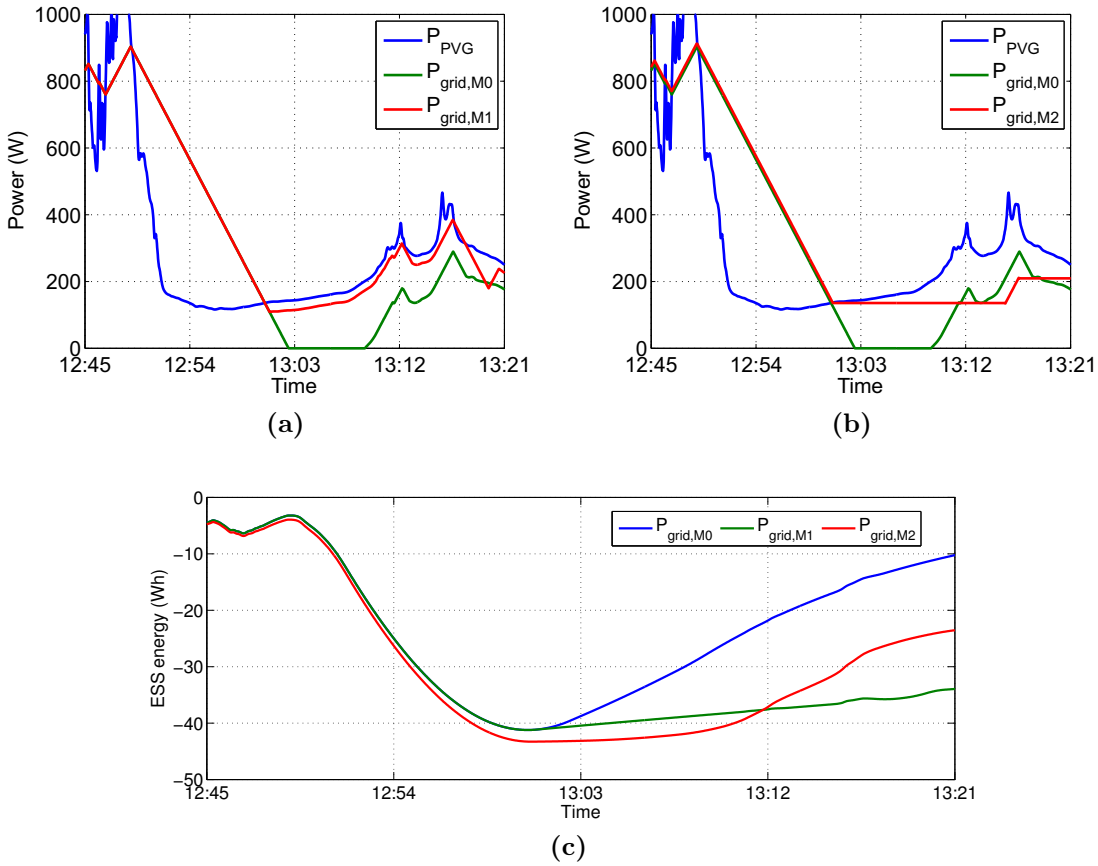

Figure 6.7. Comparison of grid feed-in behavior of Method 0 to (a) Method 1 and (b) Method 2 with (c) the resulting ESS energy evolution. Plots are from 11.07.2012 using $K = 20 \cdot 10^{-4}$ and $r = 10\ \%/\mathrm{min}$.

The second proposed method (Method 2) uses simple regulation of P_{grid} during limited downward ramps. Production outages result from downward ramps traveling below P_{PVG}. Thus, a simple rule is proposed for suspending limited downward P_{grid} to its previous value whenever $P_{\mathrm{grid}}(t - \Delta t) < P_{\mathrm{PVG}}(t)$. Figure 6.7b shows how Method 2 behaves and compares to regular SoC control. Just as Method 1, Method 2 also slows down the SoC control. Figure 6.7c displays how the ESS energy evolution with this method is balanced to its reference slightly slower than Method 0 but still much quicker than Method 1. It should be noted that this rule regulates the grid feed-in even when there is not a clear threat of outages. However, even in these cases

the method further increases P_{grid} stability by reducing the amount of fluctuations.

Unfortunately even Method 2 cannot guarantee full outage insurance. In a very similar matter as with Method 1, an outage can occur if P_{grid} regulation creates difference between very low P_{grid} and P_{PVG} values, after which a gentle downward slope has the possibility to drive P_{grid} to 0 W. Further improvement might rid both of the presented methods of the possibility of outages, but during development it was discovered that creating any additional rules to the methods could easily cause instability or SoC speed issues.

Method 2 houses also another possible problem displayed in Figure 6.8. In a situation where the regulation is applied and P_{PVG} slopes down, P_{grid} will exhibit step like behaviour below P_{PVG} (without exceeding the RR limit). These step like ramps are essentially additional fluctuations produced by the method itself. In some cases this might be seen as inadequate behaviour from the system. In practice the amplitudes of the steps are insignificantly small, and thus should not create any real problems. However, these steps are initially produced with high frequency P_{ESS} fluctuations which might not be acceptable in some practical implementations.

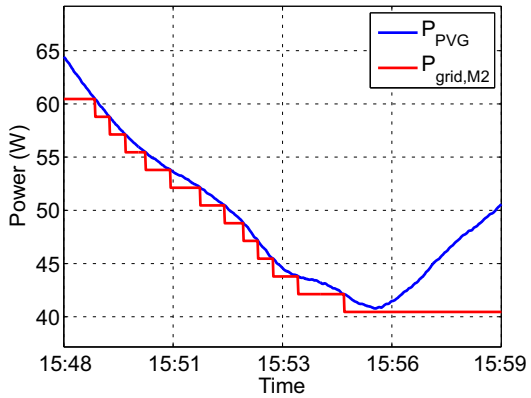

Figure 6.8. Step like behaviour in the grid feed-in power caused by the regulation in Method 2 in 11.07.2012.

6.3.3 Method Comparison

In order to know how well the proposed methods truly behave they were tested in yearlong simulations. Like in all the previous cases a 1 kWp virtual PVG with an arbitrary ESS was simulated. The following factors were monitor: required ESS capacity from Eq. 6.4, maximum ESS absolute power and the duration of yearly production outage times t_{out}. The extensive simulations were done for eight different RR limits from 1 to 50 %/min. Three different K values were used: a moderate value $5 \cdot 10^{-4}$, an optimum for most situations value $15 \cdot 10^{-4}$ and a relatively large value $20 \cdot 10^{-4}$. All the results can be seen in tables in Appendix B.

Before going into the method comparison, let us draw a few conclusions from the similarities in the results. All the methods show the same behaviour with capacity as a functions of r and K. The capacity exponentially increases with smaller RR limits regardless of K. By optimizing K for a specific r the capacity can be slightly lowered. The maximum power shows similar minimizing behaviour in respect to K optimization. In most of the cases the overall trend shows increasing maximum power for smaller RR limits, but the behaviour is somewhat case sensitive. In most of the cases the outage time trend seems to be increasing with increasing K and decreasing r.

The most notable conclusion from the comparison is that both proposed correction methods have considerably lower outage times than the original SoC control. However, Method 2 works dramatically better than Method 1 having less than one hour of outage time in all the cases and no outages at all in most of the cases. These conclusions are clearly visible in Table 6.1, which shows an extract of collected outage times using $K = 15 \cdot 10^{-4}$.

Table 6.1. Comparison of State of Charge control method outage times for different RR limits using $K = 15 \cdot 10^{-4}$ during the year 2012.

r (%/min)	1	2	5	10	20	30	40	50
$t_{\text{out,M0}}$ (h)	119.14	36.36	9.83	1.49	0.39	0.13	0.03	0.00
$t_{\text{out,M1}}$ (h)	77.30	8.84	0.08	0.00	0.00	0.00	0.00	0.00
$t_{\text{out,M2}}$ (h)	0.00	0.00	0.06	0.00	0.00	0.00	0.00	0.00

Figure 6.9 displays the C_{ESS} and $P_{\text{ESS,max}}$ comparisons between the three methods as functions of r using $K = 15 \cdot 10^{-4}$. Fig. 6.9a shows how the absolute differences in capacities are mostly marginal. The biggest relative capacity savings of 13 % can be made by choosing Method 2 when using $r = 5$ %/min. Otherwise the differences are marginal. The absolute $P_{\text{ESS,max}}$ differences in Fig. 6.9b are much more pronounced but relatively small nonetheless. In most of the cases Method 0 requires the greatest and Method 2 the least amount of power. The biggest relative power savings can be gained by choosing Method 1 with $r = 2$ %/min (12 % savings) or Method 2 with $r = 10$ %/min (9 % savings).

In conclusion of these findings Method 2 works the best on average in contrast of output quality (least amount of outages) and maximum power requirement (lowest $P_{\text{ESS,max}}$ in most cases). When also considering the marginally small absolute capacity differences between all methods, Method 2 is the clear choice for further ESS analyses.

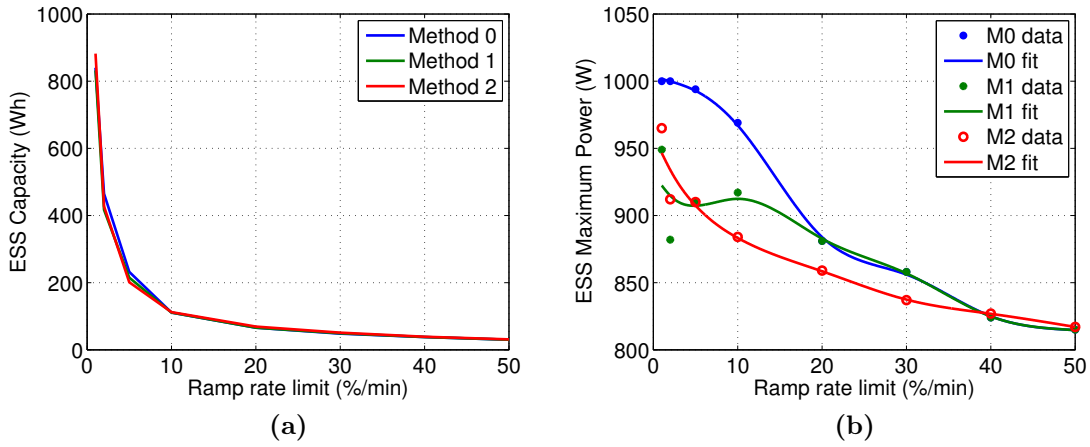

Figure 6.9. State of Charge control method comparison with (a) ESS capacity and (b) ESS maximum power as functions of the ramp rate limit using $K = 15 \cdot 10^{-4}$.

6.4 Energy Storage Sizing

Now that the required input and control matters have been defined, proper conclusions about ESS sizing can be made. Although previous chapters have already touched the subject, let us go deeper into the matter. Two major factors effect ESS sizing the most: the PVG size and the RR limit. Thus, further examinations have to be done for several different PVG sizes and varying RR limits.

Four different generator sizes were selected for closer inspection. The sizes are in the order of: 1 kWp, 100 kWp, 1 MWp and 10 MWp. Single point measurements were up-scaled using the filtering method shown in Ch. 5.1.1. When using the up-scaling method generator sizes are differentiated with the PVG area. An approximately square area was assumed to be filled with 1.5 m x 1 m 200 Wp modules placed side by side in rows with 3 meter clearance between each row as shown in Figure 6.10. With these assumptions the following areas were approximated to fit the selected generator sizes: 3,000 m^2 (100 kWp), 27,000 m^2 (1 MWp) and 0.28 km^2 (10 MWp). The small 1 kWp generator was assumed to be a tightly packed residential rooftop assembly with an area of approximately 8 m^2, which does not require the use of the spatial smoothing filter.

Using the different generator sizes and varying the RR limits between 1 and 50 %/min the one year ESS simulations were repeated and the obtained results are shown in Figure 6.11. The relative ESS capacity requirements are depicted in Figure 6.11a. Interestingly, the relative capacities are only marginally smaller for larger PVG sizes. This indicates that capacity wise it does not make a significant difference whether a cluster of smaller PVGs have their individual ESS or one central ESS, e.g. in distributed networks or sub-sections of a utility scale PVG. The ramp

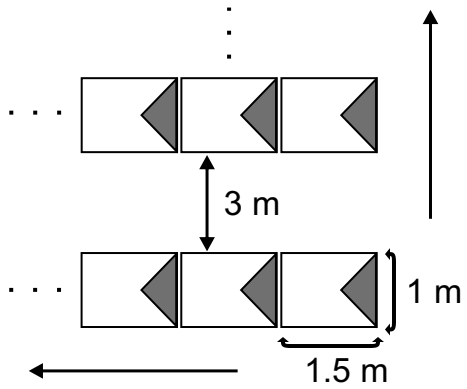

Figure 6.10. Module layout defining the virtual PVG square area for PVG upscaling.

rate limit on the other hand has a clear and exponential effect on the capacity. This is expected, as smaller RR limits are assumed to require more energy from the ESS. The exponentially decreasing behavior shows how the leniency of the grid code can drastically reduce the required ESS capacity.

The plots in Fig. 6.11b show the energy cycled through, or fed into, the ESS E_{cycled} relative to the energy fed into the grid. This information can be used to approximate possible losses associated with the ESS or the amount of utilization of the ESS. With this figure the range of values is of interest. In all examined cases the cycled energy is between 11 and 0.1 %, which indicates that utilizing an ESS would potentially cause only a small amount of losses to the energy production regardless of the RR limit, ESS size or ESS efficiency. However, with large RR limits the relative differences between PVG sizes are notable. These differences indicate that using a centralized ESS with large RR limits would cause slightly less losses.

The relative maximum power behavior in Fig. 6.11c shows more pronounced differences between PVG sizes. The larger the PVG, the less power the ESS requires relative to $P_{\text{PVG,nom}}$. The effect grows stronger with larger RR limits. This behavior is expected, since both larger PVGs and gentle RR limits are assumed to have smoother ramps, requiring less ESS peak power. These results indicate that a centralized unit could yield notable savings in the sizing of the ESS converter unit depending on the RR limit.

6.4.1 Power Rating Considerations

Let us examine the yearly ESS power behaviour more thoroughly. Thus far the focus has been in the maximum power requirement, which defines the ESS power rating if total RR limit compliance is desired. The majority of the ESS activity, however, requires only a fraction of the maximum power. For example in the simulations of the 1 kWp PVG with a RR limit of 10 %/min ESS support was required in over

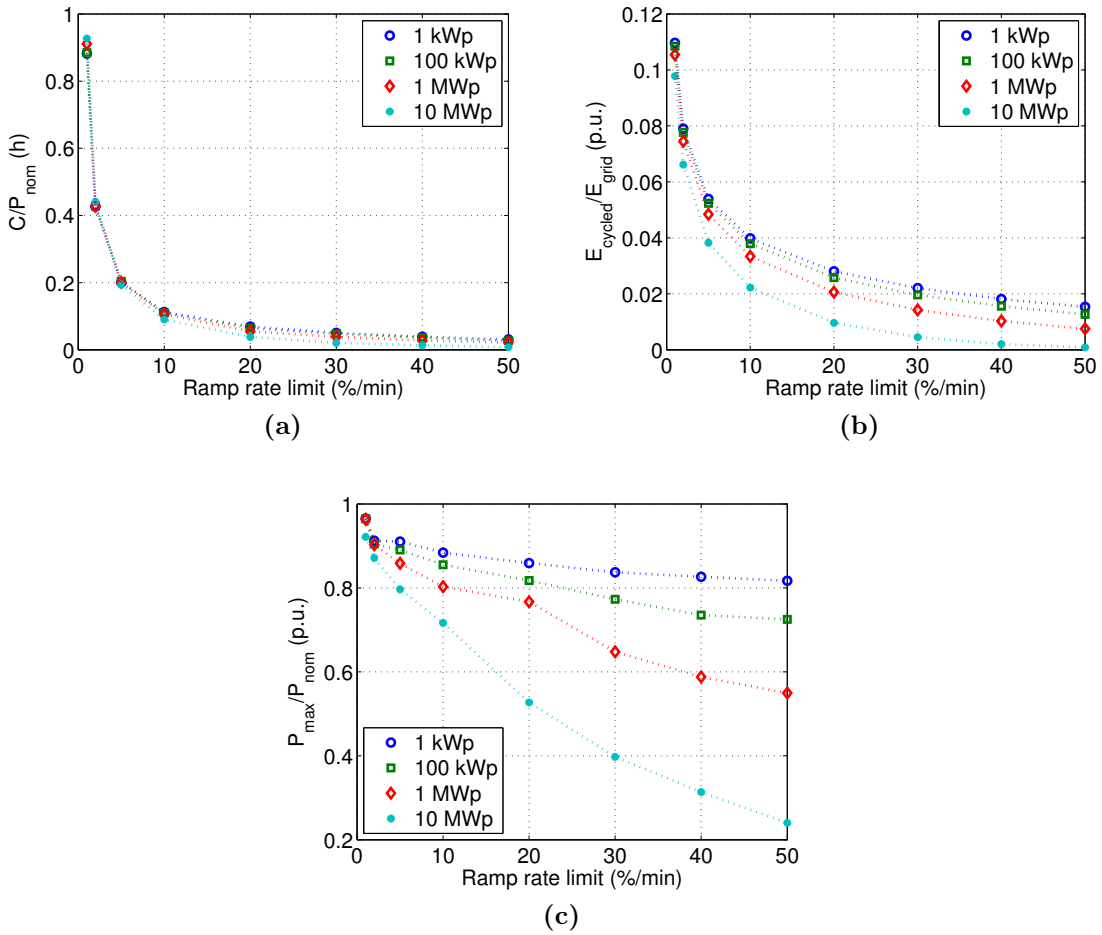

Figure 6.11. One year ESS simulation results for (a) relative capacity, (b) energy cycled through the ESS relative to total production and (c) relative maximum power. Figure (a) and (c) are relative to PVG nominal power.

100,000 occasions, lasting a combined duration of 1069 hours. Out of these the ESS would have required more than 800 W of power only on eight occasions for a total duration of less than 12 minutes. Figure 6.12 shows the usage time distribution of relative ESS power for the full year simulation of the 1 kWp and 10 MWp PVGs.

The power distributions in Fig. 6.12 reveals how the majority of ESS usage requires less than 5 % of the PVG nominal power in both cases. The use of higher power levels is drastically more marginal. The distribution stacks even more towards the lower power levels with larger PVGs. This is expected, considering the smoother PVG power behavior of larger PVGs.

These results would indicate that if the ESS user is willing to sacrifice some of the RR limit compliance then the required ESS power can be lowered. However, Figure 6.13 shows how halving the ESS maximum power alters the grid feed-in. Whenever the ESS power request is greater than it is capable of producing, partial fluctuations are fed into the grid uncompensated. Although the amplitudes of the uncompensated

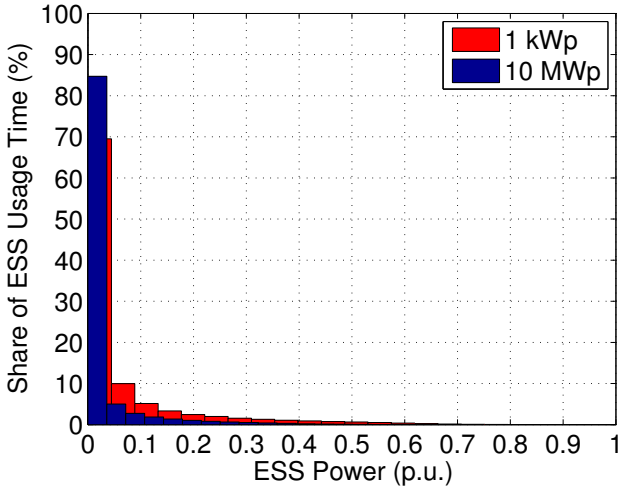

Figure 6.12. ESS power usage time distribution for (red) 1 kWp PVG and (blue) 10 MWp PVG. Power levels are relative to nominal PVG power respectively.

fluctuations are reduced, accepting such behavior is not recommended. Thus, this thesis recommends sizing the ESS based on the maximum required power $P_{\mathrm{ESS,max}}$.

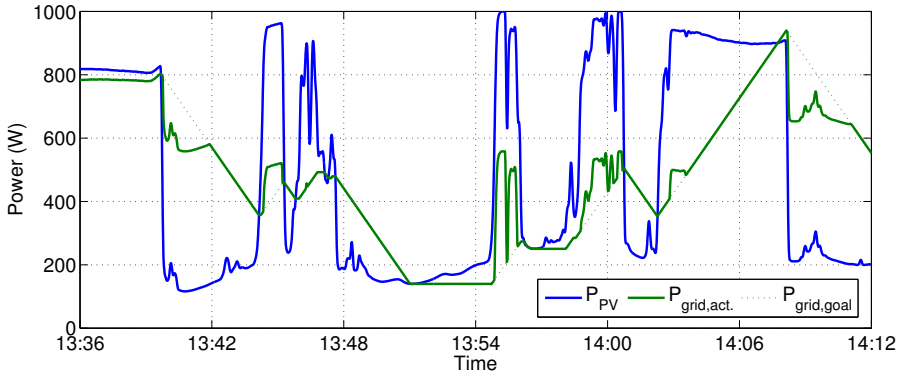

Figure 6.13. Grid feed in power behaviour with ESS power limited to half of the required level on 27.07.2012.

It should be noted that in [50] analytical formulas were presented for approximating both the required ESS maximum power and capacity for any given PVG size and RR limit. The formulas are based on theoretical requirements for compensating the worst possible PVG power fluctuations. They have been verified to produce satisfactory results compared to similar simulations as presented in this section. However, these formulas were made with the assumption that both P_{PVG} and P_{grid} change only between 10-100 % of $P_{\mathrm{PVG,nom}}$. Based on the findings in Ch. 6.3.1 this is known to be a questionable assumption, as both power terms are known to be able to go below 10 %. Essentially this assumption can lead to underestimation of the ESS power requirements especially with smaller PVGs. When comparing the results in [50] to the ones presented in this thesis the analytical formulas were found to give

similar estimations in only some of the cases. The differences could originate from different local weather conditions, the used power model or selected control method. Nonetheless, based on the observations of this thesis these analytical formulas cannot be fully recommended for all cases.

6.5 Energy Storage Cycling and Degradation

In addition to capacity and power requirements a key sizing factor is to determine a storage technology that can handle the stress that the ESS is subjected to in the fluctuation compensation application. Application induced stress can be measured with charge-discharge cycling, which degrades the ESS. With enough cycling the ESS can degrade so much that it no longer satisfies its design criteria, and has to be replaced. It is essential to map out the amount of cycling in this application, to see how much an ESS degrades and which storage technologies are suitable in this application. For the following examination batteries were chosen as an example due to their limited cycling durability. Nonetheless, the following results can be used to approximate cycling induced stress for other storage technologies as well.

In practice cycling induced degradation can be determined by counting the number of observed E_{ESS} charge-discharge cycles N. An ESS can be charged or discharged in random sequences with any amplitude between 1 and 100 % of its effective capacity. This amplitude is referred to as the Depth of Discharge (DoD). An ESS can have a different cyclelife depending on the DoD. This is especially the case with batteries, since they tend to withstand greater amounts of cycling with shallow rather than deep discharges [10, 49]. Thus, cycles have to be counted separately for each degree of the DoD. The popular Rainflow-counting algorithm was used to count the cycles this way [48]. Fig 6.14 shows the cycle counts for every given DoD N_{DoD} with varying RR limit and PVG size.

All the plots in Fig. 6.14 show a clear pattern of exponentially decreasing counts with deeper discharges. The shallowest 1 % DoD accounts for a great majority of total cycle counts. However, a large contributor to this category are the momentary E_{ESS} spikes that only slightly deviate from 0 Wh. These spikes originate from the compensation of very small or short ramps. In this thesis all factors are taken into account, but in practice some control schemes might be able to overlook these ramps. This fact somewhat diminishes the significance of this 1 % DoD category. One of the key findings in the figure is that the shallow discharges have a cycle counts in the order 100-10,000. These counts are so high that many of the storage technologies, such as lead batteries, cannot withstand them regardless of the very low energy involved with these cycles.

Figure 6.14a shows the cycle count plot for a 1 kWp PVG with three different RR limits. The figure shows a pattern of stricter RR limits inducing less cycling for the

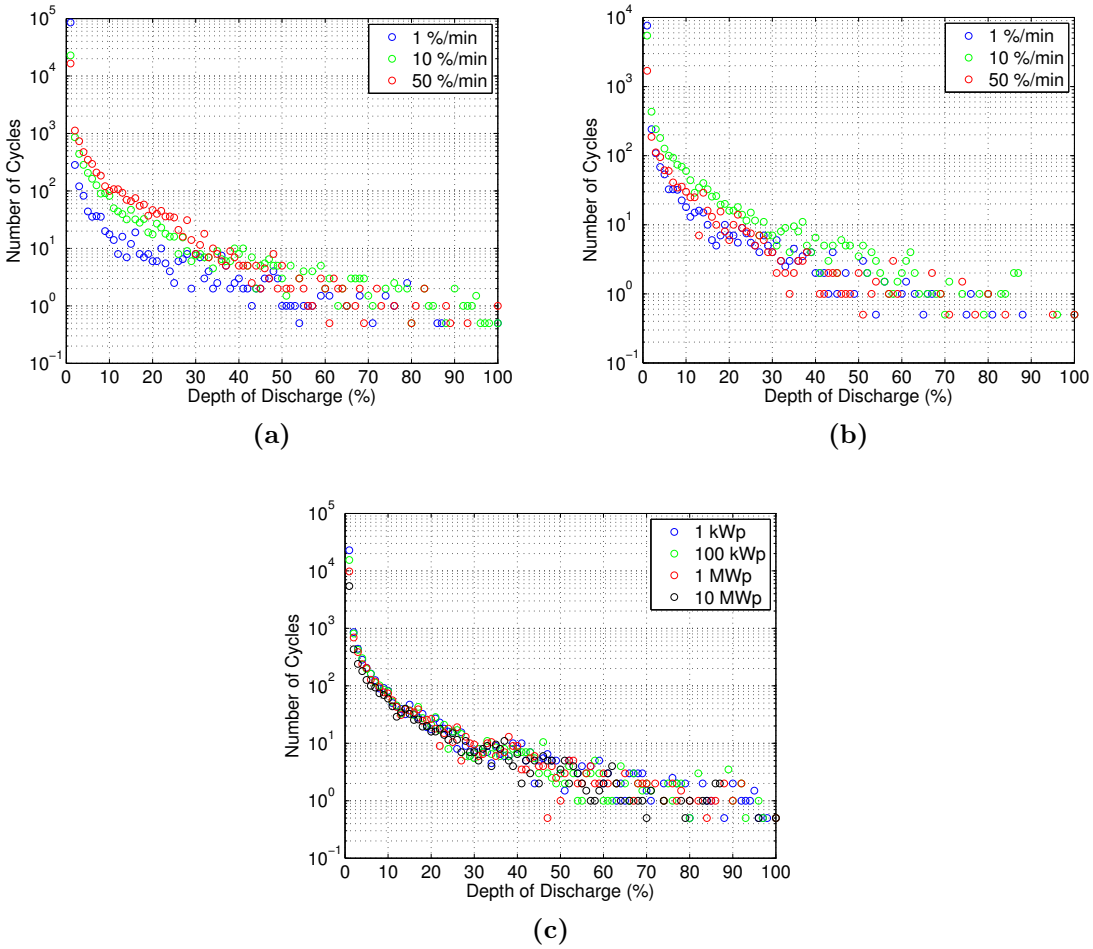

Figure 6.14. Annual cycle observations for (a) 1 kWp PVG with multiple r, (b) 10 MWp PVG with multiple r and (b) different PVGs with $r = 10$ %/min.

shallow DoDs. With deeper discharges the differences diminish as the counts overlap. Figure 6.14b shows a similar plot for a 10 MWp PVG. In this case the counts are closer together and start to overlap already with shallower DoDs. Interestingly, the mid-range RR limits have the largest amount of cycles most of the time. In both figures the 1 % DoD cycle counts show a pattern of decreasing RR limit causing more cycling.

Fig. 6.14c depicts a cycling comparison between PVG sizes with a single RR limit of 10 %/min. In the figure the counts are well overlapped throughout the plot, but even more so at shallow DoD levels. However, the 1 % DoD counts are clearly aligned in the order of PVG size. By this metric alone larger PVGs cause less cycling.

On their own the results from the cycle counting do not reveal much, since the overall effect is very unclear. For a more precise indicator of ESS degradation a comparison to a reference of the maximum cycling tolerance of the ESS is necessary.

This means that a specific ESS needs to be selected. Figure 6.15 displays an example of a cyclelife curve of a lithium-titanate battery ESS from Altairnano Technologies Incorporated [26].

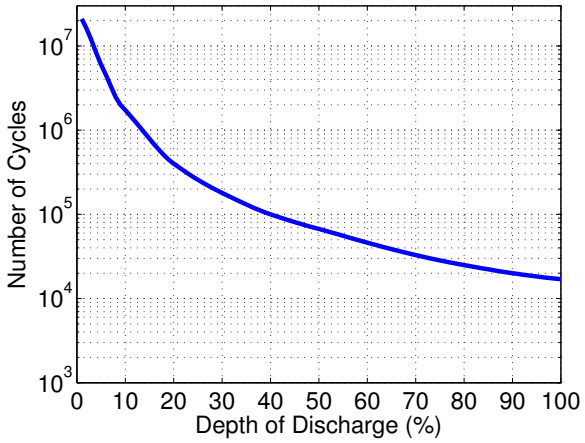

Figure 6.15. Altairnano PowerRack© lithium-titanate ESS cyclelife curve with 25 ^{o}C operating temperature adapted from [26].

The curve essentially shows the maximum amount of cycles $N_{\text{max,DoD}}$ the ESS can tolerate for a given DoD before the amount of degradation satisfies the End of Life (EoL) criteria. For batteries a typical EoL criteria is an 80 % reduction of the day-one capacity. The curve shows how the battery's tolerance has similar cycling behavior as the compensation application itself, thus indicating good compatibility. This conclusion can be extended to all battery technologies, since they have similar shapes in their cyclelife curves.

The cyclelife curve can be used as a reference to which the observed cycle counts N_{obs} from the one year simulations are compared to. The overall yearly degradation effect is calculated as the sum of each individual comparison for each DoD:

$$C_{\text{deg}} = \sum_{\text{DoD}=1\%}^{100\%} \frac{N_{\text{obs,DoD}}}{N_{\text{max,DoD}}} \cdot 100\%. \tag{6.5}$$

As an example, Table 6.2 shows the calculated annual degradation amounts for the 1 kWp and 10 MWp PVGs using an Altairnano PowerRack© with different RR limits. The table depicts very small degradation percentages, which indicates that the chosen storage model would experience very small amounts of stress in the fluctuation compensation application. It should be noted that this examination is just an example. Degradation can be more prominent for other storage systems, since lithium-titanate is an advanced technology with very high cycling tolerance. Nonetheless, the small values indicate that the application itself does not induce great amounts of degradation if the right storage technology is utilized.

Table 6.2. Annual ESS degradation for a 1 kWp and 10 MWp PVGs using different RR limits with the Altairnano PowerRack©.

r (%/min)	1	2	5	10	20	30	40	50
$C_{\text{deg, 1 kWp}}$ (%)	0.564	0.418	0.443	0.565	0.560	0.534	0.531	0.546
$C_{\text{deg, 10 MWp}}$ (%)	0.162	0.206	0.260	0.354	0.368	0.315	0.198	0.141

With both PVG sizes degradation peaks around mid-range RR limits (10-20 %). Other than that, no other RR limit related patterns were recognized. PVG size wise the results indicate that bigger generator size reduces degradation. Table 6.3 shows the annual degradation percentages for four different PVG sizes using a single RR limit. The reducing values with increasing PVG size confirm the previous conclusion. The relative figures in the table show more prominently how much the PVG size can effect the annual degradation. These results indicate that a large centralized ESS can be favorable degradation wise. It would seem that the shallowest 1 % DoD cycles, which show the most notable differences in Fig. 6.14c, can largely affect the amount of total degradation.

Table 6.3. Absolute and relative annual ESS degradation for different PVG sizes using a RR limit of 10 %/min.

$P_{\text{PVG,nom}}$	1 kWp	100 kWp	10 MWp	10 MWp
C_{deg} (%)	0.565	0.518	0.450	0.354
Rel. to 1 kWp (%)	100	98	80	64

It should be noted that even though degradation reduces the effective lifetime of the ESS, it is not the sole factor in determining how long an ESS can be used in this application. Storage systems have a calendar life, which is independent from cycling [25]. For example, if the calendar age of an arbitrary ESS would be 5 years, the annual cycling induced degradation would have to be more than 20 % for it to affect the effective operating age of the ESS. By reflecting this information to the results shown in tables 6.2 and 6.3, it is safe to say that with the right storage technology calender life becomes a bigger aging issue than cycling, regardless of the PVG size or imposed RR limit.

Another noteworthy things is that the previous examinations had a DoD swing of 1-100 % of the effective ESS capacity. Typical battery swing is limited to 20-80 % to maintain stress and to remain at the constant voltage region of the battery. This needs to be taken into account in the ESS capacity when counting cycles for an ESS with such limitations. [10, 49]

7. CONCLUSIONS

Energy storage systems have been proposed as interconnected active power compensation units for grid-connected photovoltaic generators. Their purpose is to reduce the ramp rates of fast PV power fluctuations, in order to mitigate frequency instability issues and give power system operators chance to react to these fluctuations. This thesis examined the PV fluctuation compensation application and the requirements it induced to ESS sizing and control.

ESS control and sizing analyses have been done in the past, but most of them have been based on measurement data obtained from specific PV generators. These analyses do not necessarily provide generally applicable information for ESS sizing. This thesis proposed a general modelling method that approximates PV output power through irradiance and temperature measurements. The output of the model is mainly affected by the weather conditions and not by specifications of designated PV topologies or systems. By taking spatial irradiance smoothing into account the model can be used to up-scale point sensor measurements to represent larger PVGs.

This thesis utilized a full year of data obtained from the TUT PV research plant to model virtual interconnected PV and energy storage systems. The examination of simulation results in Chapter 6 showed how downward PVG power ramps tend to require more energy for compensation than upward ramps in longer periods of time. Thus, without any additional control the required ESS energy capacity would be impractically large. The capacity can be minimized by utilizing State of Charge control.

This method, however, enables situations where the energy balancing would precede power production and cause production outages. Such behavior is not suitable for a system made to support power production. Thus, in Chapter 6 two different methods were introduced to reduce power outages while utilizing SoC. One of the methods was deemed to drastically reduce the amount of outages in all cases and even completely remove them most of the time.

ESS power and capacity requirements decrease exponentially with more lenient ramp rate limits. PVG size in turn has a marginal effect on the capacity requirements relative to the nominal PVG power. Therefore, capacity wise it does not make a difference whether a cluster of small PVGs are to have their individual ESS, or if the same cluster has one central ESS unit. Conversely to capacity, the relative ESS

power requirements depend significantly on the PVG size. The larger the PVG, the less relative power the ESS requires. The ratio of power requirement reduction depends also on the ramp rate limit. Thus, power wise centralization of the ESS can make a difference depending on the RR limit.

Total compliance of a RR limit requires the ESS to have relatively high maximum power rating. The distribution of required power, however, is heavily centered to very low power levels. If RR limit compliance can be partially sacrificed, then the ESS power rating can be drastically lowered with only occasional compliance problems.

The use of an ESS in this application requires a lot of low energy charge-discharge cycles and very few high energy cycles. Specific storage technologies can be applicable to this application if they posses a high cyclelife with very shallow cycles. With the right storage selection annual cycling induced degradation can be kept extremely low, and operation age concerns depend more on the calendar life of the ESS rather than cycling.

Ramp rate limits induce varying effects to cycling based degradation. For smaller PVGs a clear RR limit related degradation pattern does not exists. For larger PVGs the mid-range RR limits (10-30 %/min) induce the most degradation. PVG size on the other hand can have a relatively significant reduction effect to degradation. This indicates that degradation wise a large centralized storage unit would be favorable over smaller distributed units.

Concluding from all the findings of this thesis energy storage systems should first and foremost utilize a technology that can handle a great amount of cycling. Thus, Li-ion, super capacitor and flywheel technologies are recommended for instance. Due to the reduced power requirements and degradation, the ESS should rather be realized as a large centralized unit covering the needs of a large PV utility plant or a cluster or small distributed PV generators. This favors technologies that can provide large amounts of power, such as flywheels or NaS batteries. However, the benefit of a centralized unit diminishes if strict RR limits of less than 10 %/min are applied. Additionally, significant capacity reduction can be made by utilizing State of Charge control or otherwise optimizing the ESS control further.

REFERENCES

[1] B. Bose, "Global Warming: Energy, Environmental Pollution, and the Impact of Power Electronics," *IEEE Ind. Electron. Mag.*, vol. 4, no. 1, pp. 6–17, 2010.

[2] IEA, "Technology Roadmap Solar Photovoltaic Energy 2014," tech. rep., International Energy Agency, 2014.

[3] J. von Appen, M. Braun, T. Stetz, K. Diwold, and D. Geibel, "Time in the Sun," *IEEE Power Energy Mag.*, no. February, pp. 55–64, 2013.

[4] Puerto Rico Electric Power Authority, "Minimum Technical Requirements for Interconnection of Photovoltaic (PV) Facilities," tech. rep., Puerto Rico Electric Power Authority, 2012.

[5] K. Porter, "Review of International Experience Integrating Variable Renewable Energy Generation," Tech. Rep. April, Exeter Associates Inc., 2007.

[6] E.on Netz, "E.ON Netz GmbH, Grid Connection Regulations fo High and Extra High Voltage," Tech. Rep. April, E.ON Netz GmbH, 2006.

[7] Elkraft System and Eltra, "Wind Turbines Connected to Grids with Voltages above 100 kV - Technical regulation for the properties and the regulation of wind turbines," Tech. Rep. November, Elkraft System, Eltra, 2004.

[8] ISO New England Inc., "Technical Requirements for Generation - Appendix F :Wind Plant Operator Guide," tech. rep., ISO New England Inc., 2015.

[9] D. Torres Lobera, A. Mäki, J. Huusari, K. Lappalainen, T. Suntio, and S. Valkealahti, "Operation of TUT solar pv power station research plant under partial shading caused by snow and buildings," *Int. J. Photoenergy*, vol. 2013, 2013.

[10] H. Häberlin, *Photovoltaics: System Design and Practice*. John Wiley & Sons, Ltd, 2012.

[11] H. Young, R. Freedman, and L. Ford, *University Physics with Modern Physics*. Addison-Wesley, 13th ed., 2011.

[12] N. Femia, P. Giovanni, and V. Massimo, *Power Electronics and Control Techniques for Maximum Energy Harvesting in Photovoltaic Systems*. CRC Press Taylor & Francis Group, 2012.

[13] J. Carrasco, L. Franquelo, J. Bialasiewicz, E. Galvan, R. Guisado, M. Prats, J. Leon, and N. Moreno-Alfonso, "Power-Electronic Systems for the Grid Integration of Renewable Energy Sources: A Survey," *IEEE Trans. Ind. Electron.*, vol. 53, no. 4, pp. 1002–1016, 2006.

[14] D. Picault, B. Raison, and S. Bacha, "Guidelines for evaluating grid connected PV system topologies," *Proc. IEEE Int. Conf. Ind. Technol.*, vol. 2, 2009.

[15] J. Marcos, L. Marroyo, E. Lorenzo, D. Alvira, and E. Izco, "Power output fluctuations in large scale pv plants: One year observations with one second resolution and a derived analytic model," *Prog. Photovoltaics Res. Appl.*, vol. 19, pp. 218–227, Mar. 2010.

[16] R. van Haaren, M. Morjaria, and V. Fthenakis, "Empirical assessment of short-term variability from utility-scale solar PV plants," *Prog. Photovoltaics Res. Appl.*, vol. 22, no. November 2012, pp. 548–559, 2014.

[17] A. R. Dyreson, E. R. Morgan, S. H. Monger, and T. L. Acker, "Modeling solar irradiance smoothing for large PV power plants using a 45-sensor network and the Wavelet Variability Model," *Sol. Energy*, vol. 110, pp. 482–495, 2014.

[18] T. E. Hoff and R. Perez, "Modeling PV fleet output variability," *Sol. Energy*, vol. 86, no. 8, pp. 2177–2189, 2012.

[19] P. Kundur, J. Paserba, V. Ajjarapu, G. Andersson, A. Bose, C. Canizares, N. Hatziargyriou, D. Hill, A. Stankovic, C. Taylor, T. Van Cutsem, and V. Vittal, "Definition and classification of power system stability," *IEEE Trans. Power Syst.*, vol. 19, no. 3, pp. 1387–1401, 2004.

[20] S. W. Blume, *Electrical Power System Basics For the Nonelectrical Professional*. John Wiley & Sons, Ltd, 2007.

[21] E. Lorenz, J. Hurka, D. Heinemann, and H. G. Beyer, "Irradiance forecasting for the power prediction of grid-connected photovoltaic systems," *IEEE J. Sel. Top. Appl. Earth Obs. Remote Sens.*, vol. 2, no. 1, pp. 2–10, 2009.

[22] D. Lew, L. Bird, M. Milligan, B. Speer, X. Wang, E. M. Carlini, A. Estanqueiro, D. Flynn, E. Gomez-lazaro, N. Menemenlis, A. Orths, I. Pineda, J. C. Smith, L. Soder, and P. Sorensen, "Wind and Solar Curtailment," Tech. Rep. September, National Renewable Energy Laboratory, 2013.

[23] R. Y. R. Yan and T. Saha, "Power ramp rate control for grid connected photovoltaic system," *IPEC, 2010 Conf. Proc.*, pp. 83–88, 2010.

[24] B. Yang, Y. Makarov, J. Desteese, V. Viswanathan, P. Nyeng, B. Mcmanus, and J. Pease, "On the Use of Energy Storage Technologies for Regulation Services in Electric Power Systems with Significant Penetration of Wind Energy," in *5th Int. Conf. Eur. Electr. Mark. EEM*, 2008.

[25] A. Chatzivasileiadi, E. Ampatzi, and I. Knight, "Characteristics of electrical energy storage technologies and their applications in buildings," *Renew. Sustain. Energy Rev.*, vol. 25, pp. 814–830, 2013.

[26] Altair Nanotechnologies Inc., "Altairnano PowerRack Product Overview." `http://www.altairnano.com/products/powerrack/`, 2015. Accessed: 2015-06-23.

[27] ABB LTd., "Battery Energy Storage for Renewable Integration," tech. rep., ABB Ltd., 2011.

[28] Saft Groupe S.A., "Saft Li-ion energy storage smoothes grid integration for Acciona Energia's large PV power plant," tech. rep., Saft2013, 2013.

[29] Tesla Motors Inc., "Tesla Power Wall Product Overview." `http://www.teslamotors.com/powerwall`, 2015. Accessed: 2015-07-13.

[30] Xtreme Power Inc., "RAMP Series Product Overview." `http://www.xtremepower.com/product/ramp-product`, 2013. Accessed: 2015-07-10.

[31] International Renewable Energy Agency, "Battery Storage for Renewables : Market Status and Technology Outlook," Tech. Rep. January, International Renewable Energy Agency, 2015.

[32] G. Karmiris and T. Tengnér, "Control Method Evaluation for Battery Energy Storage System utilized in Renewable Smoothing," in *39th Ind. Electron. Soc.*, (Vienna), pp. 1566–1570, 2013.

[33] J. Marcos, I. n. de la Parra, M. García, and L. Marroyo, "Control Strategies to Smooth Short-Term Power Fluctuations in Large Photovoltaic Plants Using Battery Storage Systems," *Energies*, vol. 7, pp. 6593–6619, Oct. 2014.

[34] A. Ellis and D. Schoenwald, "PV Output Smoothing with Energy Storage," in *38th Photovolt. Spec. Conf. (PVSC),*, (Austin, TX, USA), pp. 1523–1528, 2012.

[35] M. Bragard, N. Soltau, S. Thomas, and R. W. De Doncker, "The balance of renewable sources and user demands in grids: Power electronics for modular battery energy storage systems," *IEEE Trans. Power Electron.*, vol. 25, no. 12, pp. 3049–3056, 2010.

[36] Z. Zheng, X. Wang, and Y. Li, "A control method for grid-friendly photovoltaic systems with hybrid energy storage units," *2011 4th Int. Conf. Electr. Util. Deregul. Restruct. Power Technol.*, no. 51007044, pp. 1437–1440, 2011.

[37] L. M. Hinkelman, "Differences between along-wind and cross-wind solar irradiance variability on small spatial scales," *Sol. Energy*, vol. 88, pp. 192–203, 2013.

[38] R. Perez, S. Kivalov, J. Schlemmer, K. Hemker, and T. E. Hoff, "Short-term irradiance variability: Preliminary estimation of station pair correlation as a function of distance," *Sol. Energy*, vol. 86, no. 8, pp. 2170–2176, 2012.

[39] K. Otani, J. Minowa, and K. Kurokawa, "Study on areal solar irradiance for analyzing areally-totalized PV systems," *Sol. Energy Mater. Sol. Cells*, vol. 47, pp. 281–288, 1997.

[40] S. Kuszamaul, A. Ellis, J. Stein, and L. Johnson, "Lanai High-Density Irradiance Sensor Network for characterizing SOLAR resource variability of MW-scale PV system," *Conf. Rec. IEEE Photovolt. Spec. Conf.*, pp. 283–288, 2010.

[41] M. Lave and J. Kleissl, "Solar variability of four sites across the state of Colorado," *Renew. Energy*, vol. 35, no. 12, pp. 2867–2873, 2010.

[42] J. Kleissl, M. Lave, M. Jamaly, and J. L. Bosch, "Aggregate solar variability," *IEEE Power Energy Soc. Gen. Meet.*, pp. 12–14, 2012.

[43] A. Longhetto, G. Elisei, and C. Giraud, "Effect of correlations in time and spatial extent on performance of very large solar conversion systems," *Sol. Energy*, vol. 43, pp. 77–84, 1989.

[44] J. Marcos, L. Marroyo, E. Lorenzo, D. Alvira, and E. Izco, "From irradiance to output power fluctuations : the pv plant as a low pass filter," *Prog. Photovoltaics Res. Appl.*, vol. 19, no. January, pp. 505–510, 2011.

[45] M. Lave, J. Kleissl, and J. S. Stein, "A wavelet-based variability model (WVM) for solar PV power plants," *IEEE Trans. Sustain. Energy*, vol. 4, no. 2, pp. 501–509, 2013.

[46] M. Garcia, L. Marroyo, E. Lorenzo, J. Marcos, and M. Pérez, "Solar irradiation and PV module temperature dispersion at a large-scale PV plant," *Prog. Photovoltaics Res. Appl.*, 2014.

[47] D. L. King, S. Gonzalez, G. M. Galbraith, and W. E. Boyson, "Performance Model for Grid-Connected Photovoltaic Inverters, SAND2007-5036," *Contract*, vol. 38, no. September, pp. 655–660, 2007.

[48] M. Chawla, R. Naik, and R. Burra, "Utility Energy Storage Life Degradation Estimation Method," in *Innov. Technol. an Effic. Reliab. Electr. Supply (CITRES), 2010 IEEE Conf.*, (Waltham, MA, USA), pp. 302–308, 2010.

[49] T. Reddy, *Linden's Handbook of Batteries*. McGraw-Hill, fourth ed., 2011.

[50] J. Marcos, O. Storkël, L. Marroyo, M. Garcia, and E. Lorenzo, "Storage requirements for PV power ramp-rate control," *Sol. Energy*, vol. 99, pp. 28–35, Jan. 2014.

APPENDIX A: DISCRETIZATION OF THE SPATIAL IRRADIANCE TRANSFER FUNCTION

Spatial irradiance filter transfer function:

$$\frac{G_{\mathrm{s}}(t)}{G(t)} = \frac{1}{(\frac{\sqrt{A}}{2\pi \cdot 0.02})s + 1} = \frac{1}{\tau s + 1}. \tag{1}$$

Using the Backward-Euler method, the Laplace-variable s is substituted with: $\frac{z-1}{zT_{\mathrm{s}}}$, where the z variable represents a step forward in time and T_{s} the sampling time. Equation 1 becomes:

$$\begin{aligned} \frac{G_{\mathrm{s}}(z)}{G(z)} &= \frac{1}{\tau(\frac{z-1}{zT_{\mathrm{s}}}) + 1} \\ &= \frac{zT_{\mathrm{s}}}{(z-1)\tau + zT_{\mathrm{s}}} \\ &= \frac{zT_{\mathrm{s}}}{z(\tau + T_{\mathrm{s}}) - \tau} \\ &= \frac{T_{\mathrm{s}}}{(\tau + T_{\mathrm{s}}) - z^{-1}\tau}, \end{aligned} \tag{2}$$

where z^{-1} represents a step back in time. Equation 2 can be implemented for example in the Matlab© using the Filter-function with the numerator and denominator depicted in the equation.

APPENDIX B: STATE OF CHARGE CONTROL METHOD COMPARISON RESULTS

Table 1. One year ESS simulation key results using Method 0.

	r (%/min)	1	2	5	10	20	30	40	50
$K = 5 \cdot 10^{-4}$	C_{ESS} (Wh)	822	502	243	162	99	66	50	39
	$P_{\text{ESS,max}}$ (W)	997	996	994	922	867	847	833	822
	Outage time (h)	60,02	20,54	2,35	0,00	0,02	0,00	0,00	0,00
$K = 15 \cdot 10^{-4}$	C_{ESS} (Wh)	840	465	232	111	66	48	38	30
	$P_{\text{ESS,max}}$ (W)	1000	1000	994	969	881	858	824	815
	Outage time (h)	119,14	36,36	9,83	1,49	0,39	0,13	0,03	0,00
$K = 20 \cdot 10^{-4}$	C_{ESS} (Wh)	936	475	237	110	60	44	35	28
	$P_{\text{ESS,max}}$ (W)	1000	1000	995	985	909	884	829	816
	Outage time (h)	147,10	41,73	12,58	2,53	0,71	0,35	0,11	0,00

Table 2. One year ESS simulation key results using Method 1.

	r (%/min)	1	2	5	10	20	30	40	50
$K = 5 \cdot 10^{-4}$	C_{ESS} (Wh)	977	502	243	162	99	66	50	39
	$P_{\text{ESS,max}}$ (W)	930	872	915	927	867	847	833	822
	Outage time (h)	48,40	3,12	0,00	0,00	0,00	0,00	0,00	0,00
$K = 15 \cdot 10^{-4}$	C_{ESS} (Wh)	832	417	215	111	66	49	38	30
	$P_{\text{ESS,max}}$ (W)	949	882	910	917	881	858	824	815
	Outage time (h)	77,30	8,84	0,08	0,00	0,00	0,00	0,00	0,00
$K = 20 \cdot 10^{-4}$	C_{ESS} (Wh)	934	422	211	110	60	46	35	28
	$P_{\text{ESS,max}}$ (W)	947	902	919	916	868	833	828	816
	Outage time (h)	88,15	11,65	0,50	0,00	0,00	0,00	0,00	0,00

Table 3. One year ESS simulation key results using Method 2.

	r (%/min)	1	2	5	10	20	30	40	50
$K = 5 \cdot 10^{-4}$	C_{ESS} (Wh)	884	502	262	167	101	70	53	42
	$P_{\text{ESS,max}}$ (W)	965	906	910	884	871	851	836	824
	Outage time (h)	0,41	0,36	0,08	0,00	0,00	0,00	0,00	0,00
$K = 15 \cdot 10^{-4}$	C_{ESS} (Wh)	882	427	201	112	69	51	39	31
	$P_{\text{ESS,max}}$ (W)	965	912	910	884	859	837	827	817
	Outage time (h)	0,00	0,00	0,06	0,00	0,00	0,00	0,00	0,00
$K = 20 \cdot 10^{-4}$	C_{ESS} (Wh)	981	449	207	108	63	47	36	29
	$P_{\text{ESS,max}}$ (W)	965	911	910	883	854	836	826	817
	Outage time (h)	0,01	0,00	0,01	0,00	0,00	0,00	0,00	0,00